<u>İSTANBUL TECHNICAL UNIVERSITY ★ INSTITUTE OF SCIENCE AND TECHNOLOGY</u>

MODELLING GROUND WAVE PROPAGATION VIA SPECTRALLY ACCELERATED METHOD OF MOMENTS (MOM) AND SPLIT STEP PARABOLIC EQUATION (SSPE)

MSc. Thesis by
Aslı Burçin NAİBOĞLU
(504031303)

Date of submission : 8 May 2006

Date of defence examination: 13 June 2006

Supervisor (Chairman): Assist. Prof. Dr. Funda AKLEMAN

Members of the Examining Committee Assoc. Prof. Dr. Selçuk PAKER (İTÜ.)

Assist. Prof. Dr. Tanju YELKENCİ (MÜ.)

JUNE 2006

İSTANBUL TEKNİK ÜNİVERSİTESİ ★ FEN BİLİMLERİ ENSTİTÜSÜ

YER DALGASI YAYILIMININ SPEKTRAL HIZLANDIRILMIŞ MOMENT METODU (MOM) VE ADIM ADIM PARABOLİK DENKLEM (SSPE) YÖNTEMLERİYLE MODELLENMESİ

Yüksek Lisans Tezi

Aslı Burçin NAİBOĞLU

504031303

Tezin Enstitüye Verildiği Tarih : **8 May 2006**

Tezin Savunulduğu Tarih: **13 June 2006**

Tez Danışmanı : **Yrd. Doç. Dr. Funda AKLEMAN**

Diğer Jüri Üyeleri: **Doç. Dr. Selçuk PAKER (İTÜ.)**

Yrd. Doç. Dr. Tanju YELKENCİ (MÜ.)

JUNE 2006

ACKNOWLEDGEMENT

I would like to express my special gratitude to my supervisor, Assist. Prof. Dr. Funda AKLEMAN, for her guidance and great helpings. This thesis wouldn't be composed without her. Also, I would like to thank Prof. Dr. Levent SEVGİ for his guidance when Mrs. Akleman was abroad for a scientific study. And at last but not at least, my special thanks to my friends and my family for their generous understanding and moral support...

July, 2006 **Aslı Burçin NAİBOĞLU**

CONTENTS

LIST OF ABBREVIATIONS

BC	: Boundary Condition
MF	: Medium Frequency
HF	: High Frequency
FBM	: Forward-Backward Method
SAFBM	: Spectrally Accelerated Forward-Backward Method
MFIE	: Magnetic Formulation of Integral Equation
EFIE	: Electric Formulation of Integral Equation
MOMI	: Method of Ordered Multiple Interactions
PEC	: Perfectly Electrical Conductor
GFBM	: Generalized Forward-Backward Method
MoM	: Method of Moments
LOS	: Line-of sight
GUI	: Guide User Interface
NLOS	: Non line-of-sight
SSPE	: Split-Step Parabolic Equation
GO	: Geometric Optics
TM	: Transverse Magnetic
TE	: Transverse Electric
EM	: Electromagnetics
UTD	: Universal Theory of Diffraction
NONPEC	: Not perfect electrically conductor
1D	: 1-Dimensional
2D	: 2-Dimensional
3D	: 3-Dimensional
IBC	: Impedance Boundary Condition
SAP	: Steepest Ascent Path
SDP	: Steepest Descent Path
FFT	: Fast Fourier Transform
PE	: Parabolic Equation
FMM	: Fast Multipole Method
TDWP	: Time Domain Wave Propagator

LIST OF TABLES

LIST OF FIGURES

LIST OF SYMBOLS

$\vec{E}$	: Electric field vector
$\vec{H}$	: Magnetic field vector
$\vec{J}$	: Electric source
$\vec{K}$	: Magnetic source
Γ	: Fresnel reflection coefficient
η	: Surface impedance
λ	: Wavelength
μ	: Magnetic permeability
ε	: Dielectric permittivity
σ	: Conductivity
γ	: Euler number
f	: Frequency
Δz	: Range step size
Δx	: Height step size
Z_0	: Free-space wave impedance
k_0	: Free-space wavenumber
ω	: Angular frequency
E_x E_y E_z	: x, y and z (cartesian coordinates) components of electric field
H_x, H_y, H_z	: x, y and z (cartesian coordinates) components of magnetic field
n	: Refractive index
X_{max}	: Maximum height

YER DALGASI YAYILIMININ SPEKTRAL HIZLANDIRILMIŞ MOMENT METODU (MOM) VE ADIM ADIM PARABOLİK DENKLEM YÖNTEMLERİYLE (SSPE) MODELLENMESİ

ÖZET

Bu çalışmada, yer dalgası yayılımı Moment Metodu (MOM) ve adım adım parabolik denklem metodu (SSPE) kullanılarak modellenmiş ve sonuçlar karşılaştırılmıştır..

Adım Adım Parabolik Denklem (Split Step Parabolic Equation, SSPE), troposferde elektromanyetik dalga yayılımında yaygın bir şekilde kullanılan bir yöntemdir. Parabolik Denklem metodu, parabolik forma indirgenmiş dalga denkleminin çözümünü sağlayan ve frekans domeninde çalışan bir yöntemdir. Tek yönlü dalga yayılımını modelleyen SSPE, eksenel doğrultuya yakın açılarda ilerleyen dalgaların modellenmesi için geçerli olup, geri yansıma etkilerini gözardı eder. Bir ilk değer problemi olan SSPE için enine başlangıç alan dağılımının bilinmesi gerekmektedir. Yayılımın başladığı mesafedeki alan dağılımı, kırılma indisi profili, $n(z,x)$, ile tanımlanan bir ortam içinde uzunlamasına (mesafe boyunca) ilerletilir ve bir sonraki mesafe için gerekli enine alan dağılımı elde edilir. Burada x ve z sırasıyla enine ve boyuna koordinatları belirtmektedir. Bu şekilde Hızlı Fourier Dönüşümü (HFD) ve Ters HFD ile x ve k_x domenleri arasında gidip gelinerek tüm uzaklıklara ilişkin enine alan profilleri hesaplanabilir. SSPE, geri saçılma etkileri az olan pürüzlü yüzeyler de dahil olmak üzere düşey ve/veya yatay olarak değişen kırılma indisine sahip ortamlarda ve özellikle VHF ile üzerindeki frekanslarda dar-bandlı dalga yayılımının modellenmesi için etkili ve güvenilir bir yöntemdir.

Moment Metodu, yaklaşık otuz yılı aşkın süredir kullanılmakta olan bir yöntemdir. Moment Metodunun ana formülasyonu, Green fonksiyonlarına bağlı olarak integral denklemi ve bu denklemin indirgenerek lineer denklem sisteminin elde edilmesine dayanmaktadır. Öncelikle ele alınan yapıya ait Green fonksiyonun analitik olarak bulunması gerekmektedir. Daha sonra, yapının yüzeyinde oluşan indüklenmiş akımlar sayısal olarak hesaplanmaktadır. Ele alınan yapının, üzerindeki akımın sabit kabul edildiği küçük parçalara ayrılması ve bu şekilde ayrık olarak elde edilen yüzey akımlarının matris sistemi şeklinde çözülmesi esasına dayanmaktadır. Akım elemanlarının sayısı ilgilenilen problemin karışıklığına göre artmaktadır ve bu sayı dogrudan matris boyutunu belirlemektedir. MoM çözümü bu matrisin tersini alma esasına dayandığı için akım elemanı sayısı arttıkça bellek gereksimi ve hesap süresi de artmaktadır.

MoM tekniği ile çözülen denklemler, elektrik alan integral denklemleri (EFIE-Electric Field Integral Equation) veya magnetik alan integral denklemleri (MFIE-Magnetic Field Integral Equation) şeklinde ifade edilmektedir. Her iki denklem de Maxwell denklemlerinin mükemmel iletken ya da dielektrikten saçılma durumunda çözülmesiyle elde edilebilmektedir. Ele alınan probleme uygun olarak bu iki tip

integral denklemden birisi seçilebilir. Her iki denklem de zaman domeninde uygulanabilir olmasına rağmen literatürde yaygın olarak frekans domeni uygulamaları bulunmaktadir.

Moment Metodu esas alınarak geliştirilen İleri-Geri yöntemiyle (İGY) bu hesaplama maliyetinin azaldığı görülmektedir. İlgilenilen problemdeki lineer denklem sistemi, yapıya ait matrisin tersini almak veya çarpanlarına ayırmak yerine, ileri ve geri yöndeki elemanları ifade etmek üzere; ele alınan matrisin alt, üst ve köşegen matrislere ayrıştırılması ile iteratif olarak çözülmektedir. Bu durumda, herbir gözlem noktasındaki akım, ileri ve geri yöndeki akımların toplamı olarak ifade edilir. Öncelikle geri yöndeki akım değerleri sıfır kabul edilir, ve bu değerler ilk iterasyonda ileri yöndeki akım değerlerini hesaplamada kulanılır. İlk iterasyonda elde edilen ileri akım değerleri de geri yöndeki akımların hesaplanmasında kullanılarak, yüzey akımları belirli bir değere yakınsayana kadar iteratif olarak hesaplama yapılır. İleri-geri yönteminin birkaç iterasyonda hızlı sonuç verdiği görülmektedir. Böylelikle, empedans matrisinin değerlerinin bellekte tutulmasına gerek olmamaktadır. Ancak ele alinan arazini profili, kaynağın yüzeyde oluşturduğu gelen alan değerleri ile matrisin köşegeni üzerindeki değerler saklanmalıdır. Böylelikle, N tane yüzey bilinmeyeni için gerekli hesaplama maliyeti N^2 olmaktadir. Daha geniş yüzeyler için hesaplama yapılırken tekrar bellek ve süre sorunuyla karşılaşılmaktadır.

İleri-Geri Yöntemini daha etkin ve hızlı hale getirmek için, Spektral Hızlandırılmış İleri-Geri Yöntemi geliştirilmiştir. Bu yöntemde, Green fonksiyonunun spektal ifadesi kullanılmakta ve matris çarpımında gerekli toplama işlemi ile integral işlemi yer değiştirmektedir. Bu sayede integral içinde kalan toplamanın her bir konum adımında yeniden yapılması gerekliliği ortadan kalkmaktadır, çünkü bir noktadaki toplam ileri ya da geri hesaba göre bir önceki ya da sonraki adımdaki toplamaya tek bir değer eklenmesi ile elde edilebilmektedir. Bu tekrarlamalı bağıntı sayesinde toplamanın getirdiği maliyet azalmaktadır. Her ne kadar integral hesabı da ek bir toplama maliyeti getirse de alınan açı elemanı sayısı akım elemanı sayısına oranla çok az olduğundan sorun yaratmamaktadır.

Bu çalışmada ileri-geri yöntemin hem SSPE hem de farklı yeryüzü şekilleri üzerinde iletimin modellenmesi için kullanılmış ve aralarında çok iyi bir uyum olduğu gözlenmiştir. Spektral hızlandırılmış MoM yönteminin geçerliliği gözlemlenmiş ve SSPE ile çözümün uygun olmadığı ortamlarda yer dalgası yayılımının modellenmesi için de kullanılabileceği gösterilmiştir.

GROUND WAVE PROPAGATION VIA SPECTRALLY ACCELERATED METHOD OF MOMENTS (MOM) AND SPLIT STEP PARABOLIC EQUATION (SSPE)

SUMMARY

In this study, ground wave propagation is modeled via Method of Moments (MoM) and Split Step Parabolic Equation (SSPE)

Split-Step Parabolic Equation (SSPE) algorithm, which is common and popular for the modeling of electromagnetic wave propagation in the troposphere, is considered. SSPE is a frequency domain wave propagator, which is the solution of a parabolic type wave equation. It is a one-way propagator that is valid under paraxial approximation (i.e., under weak longitudinal refractivity dependence or under near axial propagation), where backscatter effects are omitted. SSPE is an initial value problem and needs an initial transverse field distribution. The initial field distribution is longitudinally propagated through a medium defined by its refractive index profile, *n(z,x)* and the transverse field profile at the next range step is obtained. Here, x and z are transverse and longitudinal coordinates, respectively. By moving back and forth between x and k_x domains via Fast Fourier transforms (FFT) and inverse FFT the transverse field profile at any range may be obtained. SSPE is efficient and reliable for modeling narrow-band wave propagation (especially for frequencies VHF and above) over weakly back-scattering rough surfaces, above which exists a vertically and/or horizontally varying refractivity profile.

MoM is a very old and reliable method being used for more than three decades. Formulation of MoM is based on solving complex integral equations by reducing them to a system of linear equations. The equation solved by MoM technique is generally a form of the electrical field equation (EFIE) or magnetic field integral equation (MFIE). The form of integral equation is used determines which type of problems MoM technique is best suited for. The number of segments depends on the size of structure and the operating frequency. Increasing of matrix dimensions causes computational cost.

An iterative procedure can be used to solve forward and backward propagation equations by initializing backward currents as zero. The matrices in this iterative process do not need to be factorized or inverted. Iterations are continued until surface currents show convergence to within a specified accuracy criterion. The Forward-Backward Method has been shown to provide a more rapid convergence than a standard non-stationary iterative algorithm in many cases. In this method, the current due to the forward propagating field contribution is first found for every receiving element on the surface and then employed to recover the backward propagating field contribution in an iterative procedure. This procedure presents very accurate results within very few iterations. Using FBM, there is no need to store the elements of the impedance matrix, because of the sweeping procedure. However, the surface height data, incident field values at matching points, and forward, backward and total currents have to be stored in N element arrays, where N is the surface unknowns. Therefore, the memory requirement of the method is O(N). To make forward backward method more efficient, spectrally accelerated forward-backward method is improved. In this method, spectral representation of Green function is used and integral

operation is replaced with the sum operation used in matrix multiplying. So, addition in integral doesn’t need to be done in every range step size, because the sum at a point is obtained by adding a value to to the addition to previous or following step. By this recursive the cost of operation reduces. However, integral operation causes an increment at computation cost, but this is negligible as angle elements are less than current elements.

However, the FBM obtains an operational count of N^2 in the matrix-vector multiplication, and in order to avoid N^2 memory storage, a time-consuming computation of impedance matrix elements needs to be repeated on every iteration. This computational cost prohibits the application of the FBM to large-scale scattering problems.

In this study, Forward-Backward method has been used to model both SSPE and different terrain profiles and it has been observed that these models have a coherent between them. Accuracy of Spectrally Accelerated Forward Backward Method has been observed and it has been shown that this model can be used to model ground wave propagation where SSPE can’t be used for computation.

1. INTRODUCTION

Radio wave transmission over the earth's surface, which includes both ground and sky waves, is one of the most difficult and important propagation problems and has been a subject of interest from the beginning of the 20^{th} century. Since then, new wireless communications methods and services have been adopted by people throughout the world. The future growth of wireless communications systems will be tied more closely to radio spectrum allocations.

The frequency assignment problem has a significant role in sharing well planned frequency spectrum and obtaining the maximum serviceability. Frequency allocation and planning is a comprehensive study that implies coverage analysis, establishing locations of transmitters or receivers, computation of the interference over the candidate frequencies. Therefore, mobile radio planning requires the accurate computation of electromagnetic field strengths over large areas and in a wide variety of environments. In this regard, the problem is concerned with finding solutions and direct approaches to Maxwell's equations over randomly rough surfaces, such as integral equation based approaches.

In this work ground wave propagation modeling via SSPE (Split Step Parabolic Equation) and Spectrally Accelerated Forward Backward Method which is based on MoM (Method of Moments) is introduced to inspect the accuracy of the model.

In Chapter 2, a brief historical overview used to model ground wave propagation is given. Reflection coefficient for a smooth plane for vertical and horizontal polarization and 2-ray ground reflection modeling is mentioned. The two-ray ground reflection model considers both the direct path and a ground reflection path [1]. Besides, The Fourier Split Step algorithm used to solve parabolic type equations, common and popular for modeling electromagnetic wave propagation through troposphere is explained. The parabolic equation was firstly introduced by Leontovich and Fock in the 1940s to treat the problem of diffraction of radio waves around the earth. They used the parabolic approximation to derive more simply the well-known Watson and Van Der Pol and Bremmer results and extended the method to more complicated cases involving atmospheric refraction. Still in 1940s Malyuzhinets combined the parabolic approximation method with geometrical optics to develop a powerful theory of diffraction by obstacle. Russian workers pioneered the idea of simplifying the wave equation for certain types of radiowave equation for certain types of radiowave propagation problems and solved a number of these problems in terms of special functions. It took many years and the advent of digital computers for the parabolic approximation idea to be taken up again, this time with the aim of finding numerical solutions rather than closed-form expressions. Hardin and Tappert introduced the very efficient split-step Fourier solution of the parabolic equation for underwater acoustic problems and Claerbout developed finite-difference codes for geophysics applications. An excellent historical survey of early PE research can be found in. The finite difference implementation of the parabolic equation method provides a numerical solution to the problem of diffraction of radio waves by irregular terrain in the presence of atmospheric refraction effects [2].

In Chapter 3, ground wave propagation via MoM (Method of Moments) is explained. MoM is based on solving complex integral equations by reducing them to a system of linear equations. The equation solved by MoM technique is generally a form of the electrical field equation (EFIE) or magnetic field integral equation (MFIE). The form of integral equation is used determines which type of problems MoM technique is best suited for. The Forward-Backward Method (FBM) and spectral acceleration of this method is introduced to reduce the cost coming from matrix computations. FBM is a stationary iterative technique for solving linear system of equations resulting from electromagnetic rough surface scattering problems, which was developed for solving the magnetic field integral equation (MFIE) for perfect electrically conducting (PEC) surface by Holliday. The method has been proposed for calculating the electromagnetic current on ocean-like PEC surfaces at low grazing angles. A similar approach was developed simultaneously by Kapp and Brown and called the Method of Ordered Multiple Interactions (MOMI). Both methods provide accurate results within very few iterations, causing a computational cost and a memory requirement of N^2, where N is the number of surface unknowns [3].

Since FBM and MOMI present very fast convergence, a great number of studies have been implemented in recent years. Holliday et al. extended FBM to imperfect conductors. A curvature term was included in the propagator matrix for MOMI in order to eliminate the undesired sampling sensitivity affect. Chou and Johnson combined FBM with electric field integral equation (EFIE). Furthermore they proposed an acceleration algorithm based on the spectral representation of Green's function which reduces the operational count to *O(N)* for PEC surfaces. A combined field approach for scattering from infinite elliptical cylinders using MOMI was presented. West and Sturm investigated convergence performances and limitations of both methods by comparing them with several stationary and non-stationary iterative approaches. The FBM may not exhibit convergent behavior for surfaces where the Method of Moment (MoM) current elements are not numbered sequentially as a function of increasing x coordinate such as a ship or a large breaking wave on the ocean surface. The Generalized Forward-Backward Method (GFBM), which is a hybrid method based on a combination of the conventional FBM with MoM, was proposed to overcome this limitation in [4].

The novel spectral acceleration algorithm has been shown to produce an *O(N)* efficient iterative method of moments for the computation of radiation/scattering from both one-dimensional and two-dimensional large-scale quasi-planar structures, where N is the total number of unknowns to be solved. This method accelerates the matrix-vector multiplication in an iterative method of moments solution and divides contributions between points into *strong* (exact matrix elements) and weak (spectral acceleration algorithm) regions. The spectral acceleration is based on a spectral representation of Green functions and appropriate contour deformation, resulting in a fast multipole-like formulation in which contributions from large numbers of points to a single point are evaluated simultaneously.

Chou and Johnson extended the Spectrally Accelerated Forward-Backward Method (FBSA) formulation to treat impedance surfaces. Wang et al. applied FBM to high frequency radio wave propagation problems over forest canopies. Chou presented applications of FBM and GFBM in the analysis of large array problems. A multilevel version of the spectral acceleration algorithm was introduced. Lopez modified the spectral acceleration algorithm in order to implement FBSA to very undulating rough surfaces such as terrain profiles. The spectral acceleration algorithm was adapted to the GFBM. Çivi presented an extension of FBM with discrete Fourier transform based acceleration algorithm for the efficient analysis of large printed dipole arrays [3]. Numerical applications are given to inspect accuracy of Spectrally Accelerated Forward-Backward method by comparing Split Step Parabolic Equation.

In chapter 4, conclusions and discussions based on calculations via SSPE and Spectrally Accelerated Forward Backward Method and suggestions on future work are given.

2. GROUND-WAVE PROPAGATION MODELS

The communication path between two points above the earth's surface includes two typical wave types: ground and sky waves. Sky wave is mostly affected by the upper atmosphere (ionosphere), while ground wave is affected by the lower and middle atmosphere (troposphere) as well by the earth's surface. In this study, ground wave propagation is taken into consideration. Ground waves have three components; direct, ground-reflected and surface waves. Ground wave propagation characteristics depend on many parameters such as operating frequency, medium parameters, transmitter and receiver locations and the surface geometry with impedance effects of the ground.

The physical characteristics of the propagation depend on many parameters, such as the operating frequency, medium parameters, transmitter and receiver locations and the geometry (boundary conditions, BC) between them. Some characteristics of the ground wave propagation can be listed as: At MF and lower HF, ground wave propagation is dominated by the surface wave. As long as the transmitter and receiver are close to surface direct and ground reflected waves cancel out and only surface wave can propagate. The electrical parameters of the earth's surface play an important role in longer-range propagation. Sea surface is a good conductor, but ground is a poor conductor at these frequencies. For example, with the same transmitter and receiver characteristics, a 5MHz signal, which reaches 400 km range over the sea can only reach up to 40-50 km range over a poorly conducting ground. Typical electrical parameters of sea and ground (σ: conductivity, εr relative permittivity) are listed in Table 2.1.

In the review article of J. R. Wait [1] the ancient and modern history of EM ground wave propagation is outlined. Here we will present a brief history of the investigations related to wave propagation over the earth. For a more detailed account on this subject the reader is referred to the review paper of J. R. Wait [5].

Table 2.1 Typical ground parameters at HF

	Relative Permittivity ε_r	**Conductivity σ (s/m)**
Poor ground	4	0,001
Typical ground	15	0,005
Rich ground	25	0,02
Sea	81	5
Freshwater	81	0,001

Beginning with the original investigations of Heinrich Hertz the influence of the interference caused by the obstacles in the path had been an important subject and then in 1899 Marconi investigated the weakening of the field strength when a hill was located between transmitter and receiver. Early conjectures were that the signal was guided in some fashion by the air-earth boundary and at that time, the possible existence of the ionosphere was also broached. At the turn of the century, the presence of the earth had been a key factor to be reckoned with and this was the beginning of the subject that is now called “ground-wave propagation”.

In 1907, Zenneck analysed the possibility that the air-earth interface supported a surface wave with low attenuation. Although the guiding-wave mechanism of the air-earth interface seemed to be a leading subject to explain the radio wave transmission over long-distances, Sommerfeld took the lead to put the question on a firm mathematical basis. His analysis dealt with the problem of determining the fields of electric and magnetic dipoles located in the insulating half-space over a conducting half space as well as dipoles located in the planar interface. In 1926, Sommerfeld corrected his original formulation. In 1930s, there was an activity on the question of the validity of the Sommerfeld theory, including the modified 1926 version. Pol and Niessen confirmed that the physical form of the Sommerfeld 1926 version was correct. There has been a great deal of discussion in the literature, for the past 50 years or more, on the form that the theory should take for the general case of raised terminals. Norton developed an improved form for the Hertz potential for arbitrary heights. J. R. Wait and his former colleague, R. J. King proposed various forms that had the uniform property of reducing exactly to geometrical optics at higher elevation angles. It is pointed that Norton formulation of surface wave is to be defined as the difference between the total field and the easily computed space wave component (sum of direct and ground-reflected wave) or geometric optical field. R. J. King has also employed the surface-impedance model, in an independent integral-equation solution.

In order to deal with the actual physical world, a spherical earth model has to be used. In 1918, G. N. Watson began with the classical harmonic series solution for a dipole, in the presence of a homogeneous sphere of radius a with the electrical properties conductivity σ, dielectric permittivity ε and magnetic permeability μ. The surrounding medium was accepted as free space. Although the solution involving spherical Bessel functions of integer order was mathematically correct, convergence properties were poor. Watson's first step was to represent the series by a contour integral that enclosed the real axis of the complex wave number plane, and then he wrapped the contour around a manageable number of complex poles, which provided a highly convergent residue series in the shadow region

2.1 Reflection Coefficient for a Smooth Plane Surface

When a wave encounters a smooth plane surface, which is very large in extent, compared to a wavelength, specular reflection takes place, and the angles of incidence and reflection are equal (Snell's law) [6]. For our propagation geometry the waves move in a nearly horizontal direction, and we shall use the common terminology as follows: vertical polarization refers to linear polarization with the electric field vector lying in the vertical plane containing the incident and reflected rays and horizontal polarization refers to linear polarization with the electric field horizontal.

The relevant properties of matter are specified by a complex number, the relative dielectric constant ε_r, which is the ratio of the dielectric constant of the material to the dielectric constant of a vacuum. The complex constant ε_c, may be written as

$$\varepsilon_c = \varepsilon_r - j\varepsilon_2 \qquad \textbf{(2.1)}$$

where the imaginary part ε_2 is zero when there are no losses in the material. Alternatively, the imaginary part may be expressed in terms of the conductivity σ in mhos/meter and the wavelength λ in meters as

$$\varepsilon_2 = 60\sigma\lambda \qquad \textbf{(2.2)}$$

Complex reflection coefficients change in both vertical and horizontal cases. When the source is horizontally polarized, reflection coefficient is taken as [6]

$$\Gamma_h = \frac{(\varepsilon_r - j\varepsilon_2)\sin(\theta) - \sqrt{(\varepsilon_r - j\varepsilon_2) - \cos^2(\theta)}}{(\varepsilon_r - j\varepsilon_2)\sin(\theta) + \sqrt{(\varepsilon_r - j\varepsilon_2) - \cos^2(\theta)}} \quad \textbf{(2.3)}$$

and if the source is vertically polarized,

$$\Gamma_v = \frac{\sin(\theta) - \sqrt{(\varepsilon_r - j\varepsilon_2) - \cos^2(\theta)}}{\sin(\theta) + \sqrt{(\varepsilon_r - j\varepsilon_2) - \cos^2(\theta)}} \quad \textbf{(2.4)}$$

where θ is the angle of incidence in radians.

2.2 Ground Reflection (2-ray) Model

The 2-ray ground reflection model shown in Figure 2.1 is a useful propagation model that is based on geometric optics, and considers both direct path and ground reflected propagation path between the transmitter and receiver [7]. This model has been found to be reasonably accurate for predicting the large-scale signal strength over distance of several kilometers for mobile radio systems that use tall towers (height which exceed 50m.) as well as for line-of-sight microcell channels in urban environments.

The field strength at any observation point (i.e., at a communication receiver antenna) is due to the vector sum of all plane wave (GO ray) components which arrive at the receive point through of direct and indirect paths. A canonical example is pictured in Figure 2.1, in order to illustrate the interference between multi-path signals. In the figure, the interference effects are caused by GO rays (plane waves) that arrive the receiver via the direct and ground-reflected paths. Because of the difference in path lengths, the phases of the two rays will be different. The phases of the direct and ground-reflected rays are determined by their paths; R_{LOS}, and R_G, respectively, and they can easily be calculated from the geometry of the problem:

$$R_{LOS} = \sqrt{(h_r - h_t)^2 + d^2} \quad \textbf{(2.5a)}$$

$$R_G = \sqrt{(h_r + h_t)^2 + d^2} \quad \textbf{(2.5b)}$$

Here subscripts *r* and *t* denote receiver and transmitter, respectively and *d* is the maximum distance between the transmitter and the receiver.

If antenna heights h_t and h_r are much less than d ($d >> h_t, h_r$), surface can be assumed to be lit with grazing incidence and thus a reflection coefficient of -1. It then becomes simple to compute the vector sum of the field strengths due to the two rays, which is plotted against distance.

The resultant electric field is the sum of E-field due to the line-of-sight component at the receiver and E-field of ground-reflected ray,

$$|E_{TOT}| = |E_{LOS}| + |\Gamma E_G| \tag{2.6}$$

where Γ is the reflection coefficient for ground.

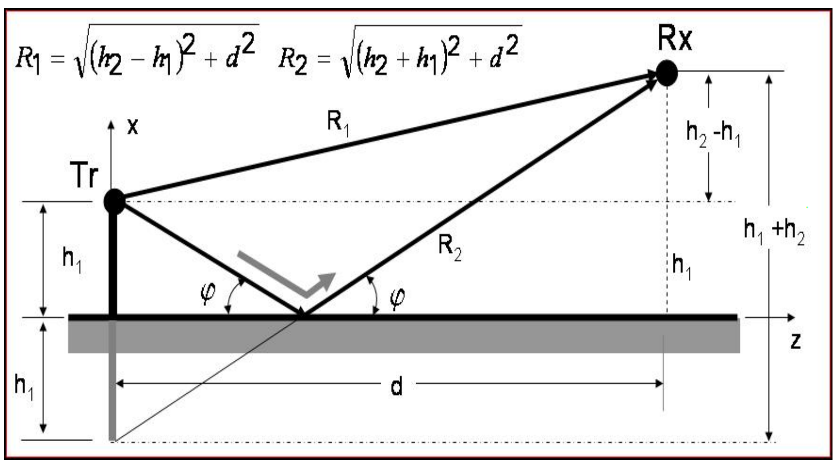

Figure 2.1 Two-ray ground reflection model

2.3 SSPE – Split Step Parabolic Equation

Parabolic equation techniques have been used extensively in radiowave propagation modeling since the mid-1980s and have become the dominant tool for assessing clear-air effects on tropospheric links. They are also increasingly applied to small-scale scattering problems such as propagation in urban environments. The parabolic equation (PE) is an approximation of the wave equation which models energy propagating in a cone centered on a preferred direction, the paraxial direction [8].

2.3.1 Parabolic Equation Framework

In all that follows, time-dependence of the fields is assumed to be $e^{-j\omega t}$ where ω is the angular frequency. Two dimensional electromagnetic field problems are concerned where the fields are independent of transverse coordinate y. There are then no depolarization effects, and all the fields can be decomposed horizontally and vertical polarized components propagating independently.

For horizontal polarization, the electric field E has only one non-zero component E_y while for vertical polarization, the magnetic field H only has one non-zero component H_y. The appropriate field component ϕ is defined by,

$$\phi(z,x) = E_y(z,x) \tag{2.7}$$

for horizontal polarization and,

$$\phi(z,x) = H_y(z,x) \tag{2.8}$$

for vertical polarization.

The wave equation is assumed to be solved in a domain where refractive index *n(z,x)* has smooth variations, assuming that suitable boundary conditions can be defined at the domain boundaries. Typically the bottom boundary is the air-ground interface and the top boundary extends to infinity. Following the convention in radiowave propagation problems, positive z-direction is chosen as propagation direction.

If the propagation medium is homogeneous with refractive index, the field component satisfies with 2-D dimensional scalar wave equation,

$$\frac{\partial^2 \phi}{\partial z^2} + \frac{\partial^2 \phi}{\partial x^2} + k_0^2 n^2 \phi = 0 \tag{2.9}$$

where k is the free-space wave number. In general, the refractive index varies with range z and height x, so equation is not exact in fact. It is however a good approximation provided the variations of n remain slow on the scale of a wavelength.

The reduced function associated with propagation direction z is obtained as,

$$\phi(z,x) = e^{-jkz} u(z,x) \tag{2.10}$$

where u denotes the wave amplitude. Point of using this reduced function is that slowly varying in range for energy propagating at angles close to propagation direction, which gives it convenient numerical properties.

The scalar wave equation in terms of u is

$$\frac{\partial^2 u}{\partial z^2} + 2jk_0 \frac{\partial u}{\partial x} + \frac{\partial^2 u}{\partial x^2} + k_0^2 (n^2 - 1)u = 0 \qquad \textbf{(2.11)}$$

This can be formally factored as,

$$\left\{\frac{\partial u}{\partial x} + jk_0(1-Q)\right\}\left\{\frac{\partial u}{\partial x} + jk_0(1+Q)\right\}u = 0 \qquad \textbf{(2.22)}$$

where Q is the pseudo-differential operator which is defined by,

$$Q = \sqrt{\frac{1}{k_0^2}\frac{\partial^2}{\partial z^2} + n^2(z,x)} \qquad \textbf{(2.13)}$$

Pseudo-differential operators are constructed from partial derivatives and ordinary functions of the variables.

The wave equation is splitted into two terms defined by Equation (2.12) and to look at functions satisfying one of the resulting pseudo-differential equations

$$u = u_+ + u_- \qquad \textbf{(2.14)}$$

$$\frac{\partial u_+}{\partial z} = -jk_0(1-Q)u_+ \qquad \textbf{(2.15)}$$

$$\frac{\partial u_-}{\partial x} = -jk_0(1+Q)u_- \qquad \textbf{(2.16)}$$

Equations (2.15) and (2.16) correspond respectively to forward and back propagating waves. In a ray picture, forward propagation corresponds to rays propagating with increasing z and backward propagation to rays propagating with decreasing z. Equations (2.15) and (2.16) are the outgoing and incoming parabolic wave equations. The standard parabolic equation for forward propagation can be easily derived using first-order Taylor expansions of the square root and exponential functions as,

$$\frac{\partial^2 u}{\partial z^2} + 2jk_0 \frac{\partial u}{\partial x} + k_0^2 (n^2 - 1)u = 0 \quad \textbf{(2.17)}$$

Equation (2.17) can also be derived with physical approximation assuming that

$$\frac{\partial^2 u}{\partial z^2} << k_0 \left| \frac{\partial u}{\partial z} \right| \quad \textbf{(2.18)}$$

And thus neglecting the term $\partial^2 u / \partial z^2$ in equation (2.11). The effect of this approximation is to neglect backscattered fields, as done in equation (2.16), and to limit accurate representation of the field to "nearly horizontal" propagation directions. When a Fourier transform is applied

$$\widetilde{u}(z, k_x) = F[u(z, x)] = \int_{-\infty}^{\infty} u(z, x) e^{-jk_x x} dx \quad \textbf{(2.19)}$$

Equation (2.17) becomes,

$$-k_x^2 \widetilde{u} + 2jk_0 \frac{\partial \widetilde{u}}{\partial z} + k_0^2 (n^2 - 1)\widetilde{u} = 0 \quad \textbf{(2.20)}$$

The solution for this first order differential equation is

$$\widetilde{u}(z, k_x) = \widetilde{u}(z_0, k_x) \exp\left[-\left(k_0^2 (n^2 - 1) + k_x^2\right)\left(z - z_0\right)/2jk_0\right] \quad \textbf{(2.21)}$$

Once the initial boundary conditions at $z=z_0$ are given, u at $z_0+\Delta z=z$ can be calculated via Equation (2.20). It should be noted that the refractive index n of the medium has been treated as a constant in the above derivation, whereas in real problems it would be a function of coordinates as *n(z,x).* To deal with such problems the step size Δz in z should be chosen, "small enough" so that within any Δz interval refractive index can be assumed to be constant with respect to z, and apply inverse Fourier transform SSPE equation to obtain

$$u(z, x) = \exp\left[j \frac{k_0}{2} (n^2 - 1)\Delta z\right] F^{-1}\left[\exp\left[-j \frac{k_x^2 \Delta z}{2k_0}\right] F\{(u(z_0, x)\}\right] \quad \textbf{(2.22)}$$

This equation can be used to calculate $u(z,x)$ along z with steps of Δz once the initial field distribution $u(z_0,x)$ is given. In numerical implementation Fourier transforms can be conveniently calculated via a fast (discrete) Fourier transform (FFT) algorithm. Since PE is an initial value problem, an initial transverse field distribution, $u(z_0,x)$ is injected then it is longitudinally propagated through a medium defined by its refractive index profile, $n(z,x)$ and the transverse field profile $u(z_0+\Delta z,x)$, at the next range step, is obtained. By sequential operations accessing the x and k_x domains via FFT and inverse FFT, respectively, one may obtain the transverse field profile at any range.

2.3.2 Standard SSPE Approach

The implementation of the SSPE algorithm is as follows [8]:

1) An initial height profile is injected into the SSPE algorithm. A 1D complex array is used to build the known (assumed) initial profile $u(z_0,x_i)$, where x_i (i=1, .., N) is the sampled height coordinate and N is the number of height points. This array contains amplitude and phase of the fields at each height.
2) The initial profile is propagated longitudinally from z_0 to $z_0+\Delta z$ via (2.22). The same complex array is used to store the height profile at the next range step.
3) Using the new height profile as the initial profile for the next step and applying the SSPE propagator for the second time yields the height profile at the second range step $z_0+2\Delta z$, etc. The procedure is applied repeatedly and vertical field profiles are stored at each range step until the propagator reaches the desired range z_{last}.
4) SSPE relies on sequential operations between the x and k_x domains, which are Fourier transform pairs. Since the transforms are implemented via discretization (i.e., via FFT) the domains are truncated at $\pm X_{max}$ and $\pm k_{xmax}$. The transverse and longitudinal step sizes Δx and Δz, respectively, and the maximum height X_{max} are determined from source and/or observation requirements as well as sampling necessities and aliasing effects. Once X_{max} is determined, k_{xmax} is found from the Nyquist sampling criteria, $X_{max} \times k_{xmax} = \pi L$, L being the transform size.

5) Because SSPE cannot handle the boundary conditions (BC) at the surface (PE defines an initial value problem) depending on whether vertically or horizontally polarized waves are of interest, one usually resorts to Dirichlet or Neumann type BCs when these can be approximated by (PEC) boundaries. These BCs can be satisfied either by extending the initial vertical profile from [$0\text{-}X_{max}$] to [$-X_{max}, X_{max}$] (odd or even symmetric), or by applying a sine or cosine FFT, respectively (An illustration is given in Figure 2.2).

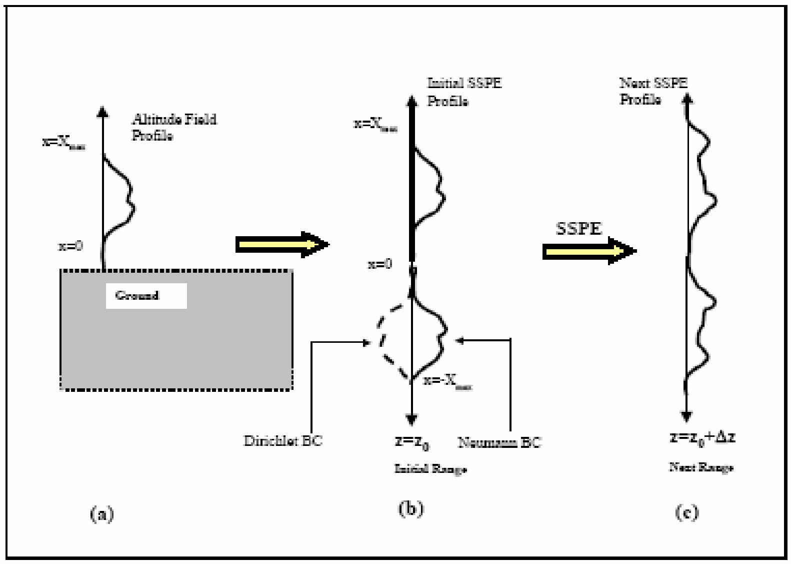

Figure 2.2 (a) The 2D propagation space that extends from x=0 to $x=X_{max}$ vertically and from $z\rightarrow -\infty$ to $z\rightarrow \infty$ horizontally. (b) Initial altitude profile of SSPE wave propagator at the range of $z=z_0$. The Dirichlet or Neumann type boundary condition at the surface is satisfied by extending vertical profile odd or even symmetric with respect to x=0 axis. The initial field profile at $z=z_0$ is $u(z_0,x)$. (c) The next altitude profile at $z=z_0+\Delta z$ is $u(z_0+\Delta z,x)$ and is obtained via a single SSPE run.

2.3.3 Non-Flat Terrain Modeling

PE modeling of propagation over irregular terrain depends on the choice of coordinate system and terrain representation, as will be discussed in this section. The simplest technique models terrain as a sequence of horizontal steps, so that sloping terrain are modeled only approximately. The staircase method is extremely effective: the grid is essentially terrain-independent so that quite large range steps can be used. More accurate modeling of slopes can be obtained by using coordinate system following terrain. A simple and effective approach introduced by represents terrain height as a continuous piecewise linear function of range, and uses a terrain-dependent reduced function [2].

2.3.3.1 Staircase Terrain Implementation

This approach models terrain with successive horizontal segments as shown in Figure 2.3. On each segments of constant height, the field is propagated in the usual way, applying the appropriate boundary condition at the ground. When the terrain height changes corner diffraction changes corner diffraction is ignored and the field is simply set to zero on vertical terrain facets. The staircase treatment is shown in Figure 2.3. if the terrain goes up, as in Figure 2.23(a), the sequence of operations to compute the field at range $z+\Delta z$ is as following:

- Propagate the field horizontal on segment S1, ignoring the presence of the vertical boundary S2. This is coherent with paraxial approximation which neglects backscatter.
- Truncate the field by setting it to zero on S2. This is coherent with the assumption that the ground does not support propagation of the wavelength of interest.

If the terrain goes down as in Figure 2.23(b), the sequence of operation is now:

- Propagate the field horizontal on segment S1, ignoring the presence of the vertical boundary S2; hence we neglect backscattering due to the corner diffraction;
- Pad the field by setting it to zero on S2.

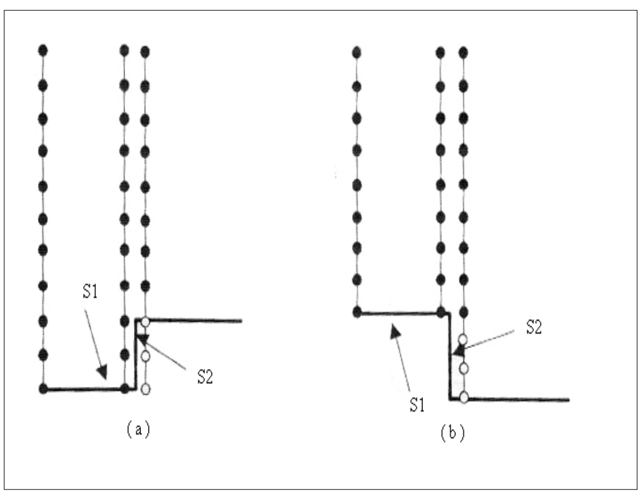

Figure 2.3 Advancing the PE solution on staircase for (a) ascending and (b) descending terrain

If the terrain was really a staircase this model would be quite accurate, extending the PE solution for half-space diffraction as described in Section 2.3.1. For smooth terrain, this representation gives erroneous results, since boundary conditions on sloping facets are not properly accounted.

2.3.3.2 Piecewise Linear Terrain Implementation

By this method terrain is represented as a sequence of linear segments, as shown in Figure 2.4. Height is measured from the terrain and new range and height variables are defined by,

$$\begin{aligned} \xi &= z \\ \zeta &= x - h(z) \end{aligned} \tag{2.23}$$

where h(z) is the terrain height with respect to range as shown in Figure (2.26).

Assuming the terrain has slope α on segment $z_1 \leq z \leq z_2$, new variables will be defined as follows in corresponding vertical slice,

$$\begin{aligned} \xi &= z \\ \zeta &= x - h(z_1) - \alpha(z - z_1) \end{aligned} \tag{2.24}$$

when these new variables are substituted into standard parabolic equation, we have this new function as defined with new variables,

$$u(z,x) = v(\zeta,\xi)\exp(j\vartheta(\zeta,\xi)) \tag{2.25}$$

If this function is substituted into equation (2.21)

$$\begin{aligned} &\frac{\partial^2 v}{\partial \xi^2} + 2j\left(\frac{\partial \vartheta}{\partial \xi} + k_0\frac{\partial \xi}{\partial \zeta}\right)\frac{\partial v}{\partial \xi} + 2jk_0\frac{\partial v}{\partial \zeta} \\ &+\left[k_0^2(n^2-1) - 2k_0\frac{\partial \vartheta}{\partial \zeta} - 2k_0\frac{\partial \vartheta \partial \xi}{\partial \xi \partial \zeta} + j\frac{\partial^2 \vartheta}{\partial \xi^2} - \left(\frac{\partial \vartheta}{\partial \xi}\right)^2\right]v = 0 \end{aligned} \tag{2.26}$$

will be obtained.

Then the modified PE equation is obtained as

$$\frac{\partial^2 v(\zeta,\xi)}{\partial \xi^2} + 2jk_0\frac{\partial v(\zeta,\xi)}{\partial \zeta} + k_0^2\left(n^2\left(\zeta,\xi + h(\zeta)\right) - 1 - 2\xi h''(z)\right)v(\zeta,\xi) = 0 \tag{2.27}$$

where

$$v(\zeta,\xi) = u(z,x)\exp\left[-j\left[k_0\xi h'(\zeta) + \frac{3}{2}k_0\int_0^{\zeta} h'(\beta)d\beta\right]\right] \quad \textbf{(2.28)}$$

with the term in the brackets representing the final form of the function ϑ. Here, $h'(\zeta)$ and $h''(\zeta)$ denote first and second derivatives of the terrain height function with respect to ζ, respectively.

If the terrain function is known, it is easy to apply this conformal mapping to the SSPE algorithm since only the second derivative of the function is needed. But terrain function is rarely available; instead, ground height difference with range can be measured. Therefore only the terrain height for each range step can be assumed to be known. With the help of this information, terrain can be represented as a sequence of linear segments.

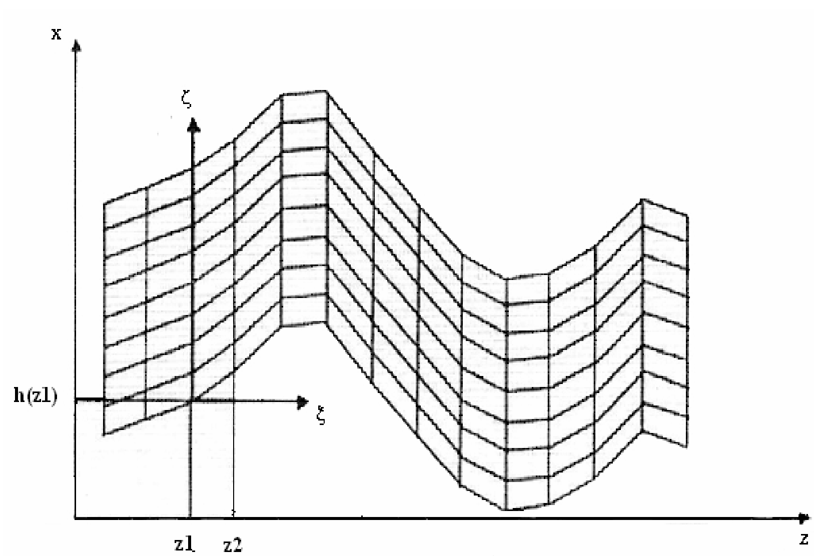

Figure 2.4 Modified coordinate system for linear terrain

Although staircase terrain cannot model the terrain as smooth as it must be (see Figure 2.5), comparisons show that the results are quite satisfactory (see Figure 2.7).

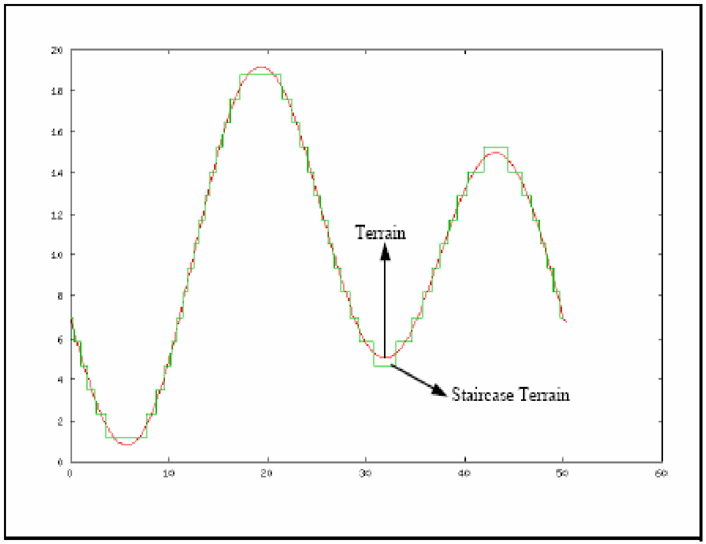

Figure 2.5 The difference between terrain and its staircase approximation

2.3.4 SSPE Algorithm

In Figure 2.6 classical SSPE algorithm is given and implementation steps are listed in Section 2.2.2 the program starts with the user supplied initial vertical scalar field profile, some parameters (such as frequency, maximum height, first range, last range, range increment) and vertical refractivity profile that may also be range-dependent. Transverse field profile may be obtained at any range by applying one forward and one backward FFT. FFT and inverse FFT in x and k_x domains respectively. After each run, the program checks if the last range is reached. If not program continues running for next range. At each range new calculated new profile is replaced. At last range, output is written, for our program propagation factor and path loss in dB is plotted vs range.

2.3.5 Numerical Applications

For a more detailed account on this subject the reader is referred to [21].

Staircase and piecewise linear approximations are tested against various propagation scenarios that include non-flat terrain profiles. In Figure 2.7, a double hill concave-convex type terrain is chosen and path loss vs. range at 15m above the ground is calculated. Transmitter is located at 15m and maximum range of 60 km is considered. Both staircase and piecewise linear terrain SSPE algorithms, give similar results. The ripples in the staircase result are because it cannot model the terrain as smooth as it must be.

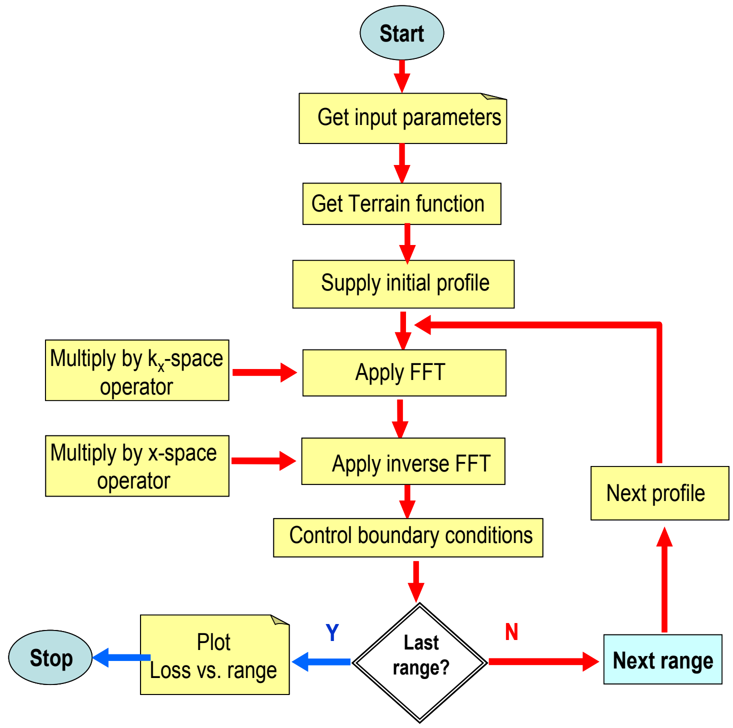

Figure 2.6 Flowchart for classical SSPE algorithm

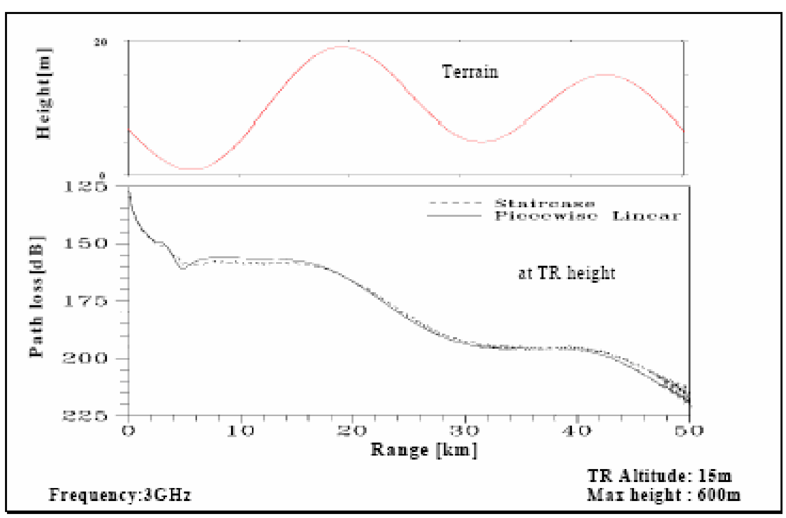

Figure 2.7 Top: Concave-convex type terrain Bottom: The comparison of path loss calculated with staircase and piecewise linear terrain implementations

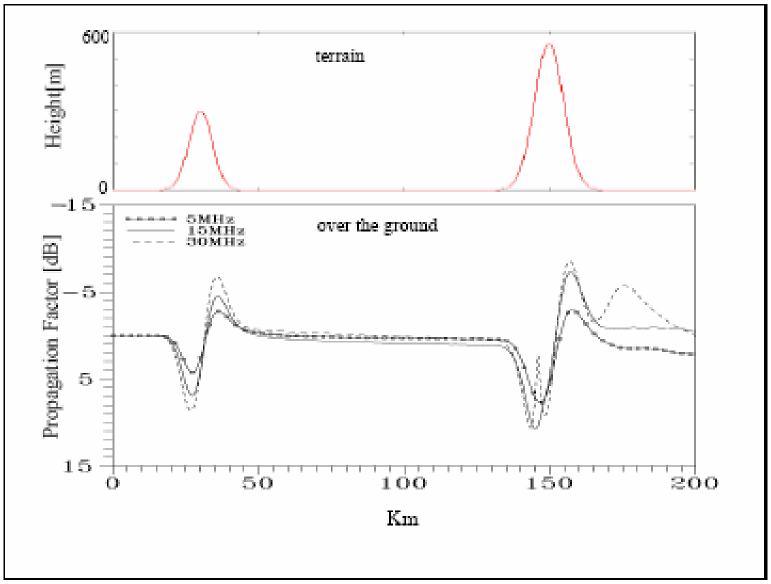

Figure 2.8 EM propagation over a typical terrain, which can be accepted as two mountains, with a valley in between, is modeled for three different frequencies, 5, 15 and 30MHz.

Then a two- hill scenario is chosen as pictured in Figure 2.8. A 300 m and 500 m hills, separated approximately by a distance of 120km is taken into account and propagation is simulated via piecewise linear SSPE. The results are plotted as propagation factor vs. range at three different (5, 15, 30 MHz) frequencies in the high frequency (HF) band. Therefore, only for this comparison, propagation factor P_f is defined as, E_t and E_g denoting the electric field values at a given point over PEC terrain and PEC ground without terrain, respectively. In order to calculate P_f, SSPE is run twice and in the first run, propagation over PEC terrain is simulated. In the second run, it is repeated for PEC ground without terrain and the propagation factor, which includes only the terrain effects, is obtained. The higher the frequency the more terrain influence on propagation is seen in the figure.

3. RADIOWAVE PROPAGATION ANALYSIS: METHOD OF MOMENTS (MOM) SOLUTION

3.1 The Methods of Moment Solution

The basic idea is to reduce a functional equation to a matrix equation, and then solve the matrix equation by known techniques. These concepts are best expressed in the language of linear spaces and operators. [9]

Most EM problems can be stated in terms of an inhomogeneous equation

$$L(f) = g \qquad \textbf{(3.1)}$$

where L is an operator which may be differential, integral or integro-differential, g is the known excitation or source function, and f is the unknown function to be determined.

The *method of moments* (MOM) is a general procedure for solving equation (3.1). The method owes its name to the process of taking moments by multiplying with appropriate weighing functions and integrating. In western literature, the first use of the name is usually attributed to Harrington [10]. The origin and development of the moment method are fully documented by Harrington [11, 12]. The method of moments is essentially the method of weighted residuals as discussed [Section 4.6, 13]. Therefore, the method is applicable for solving both differential and integral equations.

The use of MOM in EM has become popular since the work of Richmond in 1965 and Harrington [14] in 1967. The method has been successfully applied to a wide variety of EM problems of practical interest such as radiation due to thin-wire elements and arrays, scattering problems, analysis of microstrips and lossy structures, propagation over an inhomogeneous earth, and antenna beam pattern, to mention a few. An updated review of the method is found in a paper by Ney [13]. The literature on MoM is already so large as to prohibit a comprehensive bibliography. A partial bibliography is provided by Adams [15].

The procedure for applying MoM to solve equation (3.1) usually involves four steps:

(1) derivation of the appropriate integral equation

(2) conversion (discretization) of the integral equation into a matrix equation using basis (or expansions) functions and weighting (or testing) functions

(3) evaluation of the matrix elements

(4) solving the matrix equation and obtaining the parameters of interest

If we expand f in a series of functions $u_1, u_2, u_3, \ldots$ in the domain of L, as

$$f = \sum_n \alpha_n u_n \tag{3.2}$$

where α_n are constants. u_n is called as expansion functions or basis functions. For exact solutions equation (3.2) is usually an infinite summation and the u_n form a complete set of basis functions. For approximate solutions, equation (3.2) is usually a finite summation. Substituting (3.2) into (3.1) and using the linearity of L, we have

$$\sum_n \alpha_n L(u_n) = g \tag{3.3}$$

It is assumed that a suitable inner product $<u, g>$ has been determined for the problem. As next, a set of weighting functions or testing functions $w_1, w_2, w_3, \ldots$ in the range of L are defined and inner product of (3.3) is taken with each w_m. As a result,

$$\sum_n \alpha_n \langle w_m L.u_n \rangle = \langle w_m, g \rangle \tag{3.4}$$

is obtained. Here m is an integer starting from 1 to a finite number *(m=1,2,3,…)*

This set of equations can be written in matrix form as

$$[l_{mn}][\alpha_n] = [g_m] \tag{3.5}$$

where

$$[l_{mn}] = \begin{bmatrix} \langle w_1 Lf_1 \rangle & \langle w_1 Lf_2 \rangle & \ldots \\ \langle w_2 Lf_1 \rangle & \langle w_2 Lf_2 \rangle & \ldots \\ \ldots & \ldots & \ldots \end{bmatrix} \tag{3.6}$$

$$[\alpha_n] = \begin{bmatrix} \alpha_1 \\ \alpha_2 \\ \vdots \end{bmatrix} \qquad [\alpha_n] = \begin{bmatrix} \langle w_1, g \rangle \\ \langle w_2, g \rangle \\ \vdots \end{bmatrix} \tag{3.7}$$

If the matrix [***l***] is nonsingular its inverse exists. The α_n is then given by

$$[\alpha_n] = [l_{mn}^{-1}][g_m] \tag{3.8}$$

And solution for f is given by equation (3.2). For concise expression of this result, the matrix form of functions are defined as,

$$[\widetilde{u}_n] = [u_1 \quad u_2 \quad u_3 \quad \ldots] \tag{3.9}$$

and

$$f = [\widetilde{u}_n][\alpha_n] = [\widetilde{u}_n][l_{mn}^{-1}][g_m] \tag{3.10}$$

can be written.

This solution may be exact or approximate depending upon the choice of the u_n *a*nd w_n.

If the matrix [*l*] is of infinite order, it can be inverted only in special cases for example if it is diagonal. The classical eigenfunction method leads to a diagonal matrix, and can be thought of as a special case of the method of moments. If the sets u_n and w_n are finite, the matrix is of finite order, and can be inverted by known methods. [10, appendix B]

One of the main tasks in any particular problem is the choice of the u_n and w_n. The u_n should be linearly independent and chosen so that some superposition (3.2) can approximate f reasonably well. The w_n should also be linearly independent and chosen so that the products $\langle w_n, g \rangle$ depend on relatively independent properties of g. Some additional factors which affect the choice of u_n and w_n are,

1. The accuracy of the solution desired
2. The ease of evaluation of the matrix elements
3. The size of the matrix that can be inverted
4. The realization of a well-conditioned matrix [*l*]

Point Matching

The integration involved in evaluating is often difficult to perform in problems of practical interest. A simple way to obtain approximate solutions is to require that equation (3.3) be satisfied at discrete points of region of interest. This procedure is called as *point matching method/* In terms of the method of moments, it is equivalent to using Dirac delta functions as testing functions.

3.2 Ground Wave Propagation Modeling via MoM

Ground-wave propagation problem can be analyzed in 2-D medium. Harmonic time convention is assumed as and suppressed throughout. Modeling of problem geometry for the rough surface is illustrated in Figure 3.1 and can be obtained by electric and magnetic sources, $\vec{J}$ and $\vec{K}$, respectively.

$$\vec{J} = \hat{n} \times \vec{H} \quad \textbf{(3.11)}$$

$$\vec{K} = \vec{E} \times \hat{n} \quad \textbf{(3.12)}$$

Here $\vec{H}$ and $\vec{E}$ are electric and magnetic fields respectively.
Since the relative permittivity is large, the equivalent source of (3.11) and (3.12) can satisfy the impedance boundary condition (IBC) on the surface

$$\vec{K}(\rho) = \eta_s(\rho) \cdot \vec{J}(\rho) \times \hat{n}(\rho)$$

(3.13)

where η_s denotes the surface impedance, which may vary along the surface and $\hat{n}$ denotes the unit normal vector to the surface.

An arbitrary electro-magnetic field can be expressed as the sum of transverse magnetic part (TM) and a transverse electric part (TE) part. The TM part has only components of magnetic field *H* transverse to y and TE part has only components of *E* transverse to *y*. For two-dimensional fields in isotropic media, the TM part has only y component of *E* and TE part has only y component of *H*. In many cases TE and TM parts can be treated separately, reducing the problem to a scalar problem. In following sections TE and TM cases will be examined respectively.

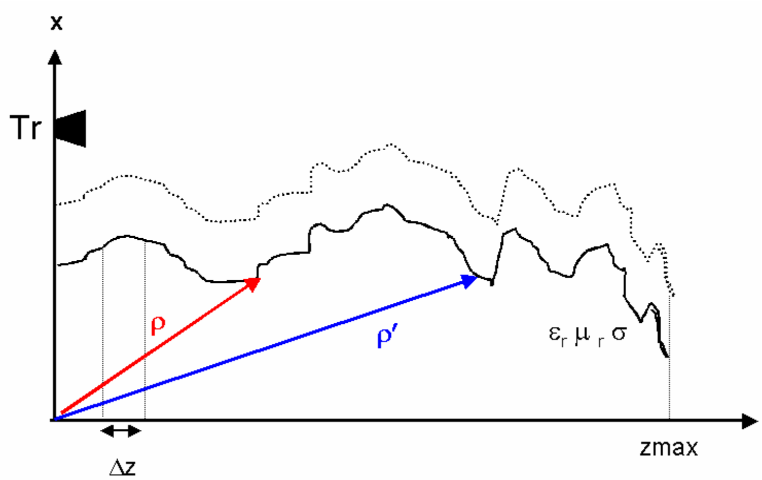

Figure 3.1 Problem geometry

3.2.1 Vertical Polarization (TE) Case

To compute the scattered field, unknown current induced on the surface has to be obtained for a given incident field. When the incident field has a vertical polarization magnetic field vector is used, and if an impedance boundary condition is valid along the surface,

$$K_y(\rho) = -E_t(\rho) = \eta_s(\rho)H_y(\rho) = -\eta_s(\rho)J_t(\rho) \qquad \textbf{(3.14)}$$

According to MFIE formulation, the magnetic field integral equation is valid on the scattering surface as

$$-H_y^{inc}(\rho) = J_t(\rho) + H_y^{scat}(\rho) \qquad \textbf{(3.15)}$$

where J_t is the tangential induced current.

Scattered magnetic field can be expressed as a function of the magnetic and electric vector potentials, which are integrals of two-dimensional Green's functions.

$$\begin{aligned} -H_y^{inc}(\rho) = J_t(\rho) + j\omega\varepsilon \int_C \eta_s(\rho')J_t(\rho')G(\rho,\rho')d\rho' \\ - \int_C J_t(\rho')\frac{\partial}{\partial n'}G(\rho,\rho')d\rho' \end{aligned} \qquad \textbf{(3.16)}$$

where ε and μ are the permeability and permittivity of the medium above the rough surface, respectively. G is the two-dimensional Green's function, and $\frac{\partial}{\partial n'}G$ is its derivative respect to $\hat{n}'$, the normal vector to the surface at the source point ρ'. Green's function is expressed as,

$$G(\rho,\rho') = \frac{1}{4j} H_0^{(2)}(kR) \quad \textbf{(3.17)}$$

where $H_0^{(2)}$ is the second kind Hankel function with order two and,

$$R = \sqrt{[x(\rho) - x(\rho')]^2 + [z(\rho) - z(\rho')]^2} \quad \textbf{(3.18)}$$

Also as illustrated in Figure 3.1, in Equation (3.18) primed coordinates denote the source locations, while unprimed coordinates represent observation points on the terrain surface. So *R* denotes the distance of the source and observation locations from the origin.

The current density $J_t(\rho)$ radiates in free-space and generates the scattered fields. This equation is to be solved through discretization by using the method of moments (MoM).

Surface length is approximated by *N* tilted straight segments of horizontal width Δz. By employing a unit pulse basis function on each segment, induced current density at observation points can be represented by,

$$J_t(\rho') \cong \sum_{m=1}^{N} I_m p_m(\rho') \quad \textbf{(3.19)}$$

where $p_m(\rho')$ denotes the unit pulse-basis function centered on the *m*th segment and I_m is its associated coefficient. These current coefficients, are used to obtain incident magnetic fields at observation points on the surface,

$$\begin{aligned} -H_y^{inc}(\rho_n) = I_n &+ j\omega\varepsilon \sum_{m=1}^{N} I_m \int_{\Delta z} \eta_s(\rho_m) G(\rho_n,\rho_m) d\rho' \\ &- \sum_{m=1}^{N} I_m \int_{\Delta z} \frac{\partial}{\partial n'} G(\rho_n,\rho_m) d\rho' \end{aligned} \quad \textbf{(3.20)}$$

where ρ_n denotes the observation point located on the center of the nth segment on the terrain surface and ρ_m the source point of the *m*th.

In order to obtain a solution for these *N* amplitude constants, *N* linearly independent equations are necessary.

$$-\begin{bmatrix} H_y^{inc}(\rho_1) \\ H_y^{inc}(\rho_2) \\ \vdots \\ H_y^{inc}(\rho_N) \end{bmatrix} = \begin{bmatrix} Z_{11} & Z_{12} & \cdots & Z_{1N} \\ Z_{21} & Z_{22} & \cdots & Z_{2N} \\ \vdots & \vdots & \cdots & \vdots \\ Z_{N1} & Z_{N2} & \cdots & Z_{NN} \end{bmatrix} \begin{bmatrix} I_1 \\ I_2 \\ \vdots \\ I_N \end{bmatrix} \tag{3.21}$$

or

$$[V_n] = [Z_{nm}][I_m] \tag{3.22}$$

The entries of the MoM impedance matrix in (3.21) is given by,

$$Z_{nm} = \int_{\Delta z} \left[j\omega\varepsilon\eta_m G(\rho_n, \rho_m) - \frac{\partial}{\partial n_m} G(\rho_n, \rho_m) \right] d\rho' \tag{3.23}$$

If the segments are small compared to the wave-length, about λ/10, the elements of the impedance matrix may be approximated as,

$$Z_{nm} \cong \frac{\omega\varepsilon\eta_m}{4} \Delta z H_0^{(2)}(k|\rho_n - \rho_m|) + j\frac{k}{4} \Delta z H_1^{(2)}(k|\rho_n - \rho_m|)\hat{n}_m . \hat{\rho}_{nm} \tag{3.24}$$

where *Δz* is length of one segment, and η_m is the surface impedance for each segment, ω is the radial frequency, ε is the permittivity of the medium. $H_1^{(2)}$ and $H_0^{(2)}$ are the second-kind Hankel functions with order one and with order two, respectively. Also, $\hat{n}_m$ denotes the unit normal vector of the surface at ρ_m and $\hat{\rho}_{nm}$ denotes the unit vector in the direction from source ρ_m to the receiving element ρ_n.

Since the Hankel function is singular for $\rho_n=\rho_m$, diagonal entries of the impedance matrix are obtained as;

$$Z_{mm} \cong \frac{1}{2} + \frac{\omega\varepsilon\eta_m}{4} \Delta z \left[1 - j\frac{2}{\pi} \ln\left(\frac{\gamma k \Delta z}{4e} \right) \right] \tag{3.25}$$

Here, γ denotes Euler number which is equal to 1,781072418 and e is equal to 2,718281828 exactly.

As a result of MoM procedure, $N \times N$ sized impedance matrix is generated, resulting in an $O(N^2)$ computational algorithm that becomes intractable for large rough surface sizes.

Once impedance matrix is obtained $V = \overline{Z} \cdot I$ should be solved for induced current coefficients, I_m, to compute scattered fields. Direct solution to MoM algorithm costs $O(N^3)$ operations, therefore instead of MoM, an iterative method called forward-backward method (FBM) can be used.

The elements of the vector V, initial voltage on the surface, are taken as;

1. When the incident field is a finite plane wave,

$$V_n = -H_y^{inc}(\rho_n) = \frac{1}{\eta_0}\begin{cases} e^{-jk(z_n\cos\theta - x_n\sin\theta)} & ,if \quad 0 < z_n < z_{\max} \\ 0 & ,otherwise \end{cases} \tag{3.26}$$

2. When the terrain is illuminated by an isotropic radiator such like a point source,

$$V_n = -H_y^{inc}(\rho_n) = -\frac{E_0}{\eta_0}\frac{e^{-jkd_n}}{d_n} \tag{3.27}$$

E_0 is the magnitude of the electric field related to the transmitted power from the isotropic radiator in,

$$E_0 = \sqrt{60P_t} \tag{3.28}$$

$$d_n = \sqrt{\left[x(\rho_n) - x_{source}\right]^2 + \left[z(\rho_n) - z_{source})\right]^2} \tag{3.29}$$

where x and z denotes the height and range locations, respectively, of the observation points on the surface where the scattered field will be calculated and the electromagnetic source location.

3. When the terrain is illuminated by an infinitesimal dipole,

$$V_n = -H_y^{inc}(\rho_n) = -\frac{E_0}{\eta_0}\frac{e^{-jkd_n}}{d_n}\sin\theta_n \tag{3.30}$$

$$\sin\theta_n = \frac{z(\rho_n) - z_{source}}{d_n} \tag{3.31}$$

4. When the terrain is illuminated by a line source,

$$V_n = -\frac{j}{4} H_0^2(k\rho_n) \tag{3.32}$$

where $H_0^{(2)}$ denotes the second kind Hankel function with order two.

3.2.2 Horizontal Polarization (TM) Case

As the same way given to derive MFIE in section 3.1.1, EFIE can be obtained. In horizontal polarization, polarization electric field component E_y is used, and if an impedance boundary condition is valid along the surface,

$$K_t(\rho) = E_y(\rho) = \eta_s(\rho) H_t(\rho) = \eta_s(\rho) J_y(\rho) \tag{3.33}$$

According to EFIE formulation, the electric field integral equation is valid on the scattering surface as

$$-E_y^{inc}(\rho) = \eta_s J_y(\rho) + E_y^{scat}(\rho) \tag{3.34}$$

where J_y is the surface electrical current.

Scattered electric field can be expressed as a function of the magnetic and electric vector potentials, which are integrals of two-dimensional Green's functions.

$$\begin{aligned} -E_y^{inc}(\rho) = -\eta_s(\rho) J_t(\rho) - j\omega\mu \int_C J_y(\rho') G(\rho,\rho') d\rho' \\ + \int_C \eta_s(\rho') J_y(\rho') \frac{\partial}{\partial n'} G(\rho,\rho') d\rho' \end{aligned} \tag{3.35}$$

where ε and μ are the permeability and permittivity of the medium above the rough surface, respectively. G is the two-dimensional Green's function, and $\frac{\partial}{\partial n'} G$ is its derivative respect to $\hat{n}'$, the normal vector to the surface at the source point ρ'. Surface length is approximated by N tilted straight segments of horizontal width Δz. By employing a unit pulse basis function on each segment, induced current density at observation points can be represented by,

$$J_y(\rho') \cong \sum_{m=1}^{N} I_m p_m(\rho') \tag{3.36}$$

where $p_m(\rho')$ denotes the unit pulse-basis function centered on *m*th segment and I_m is its associated coefficient. These current coefficients, are used to obtain incident magnetic fields at observation points on the surface,

$$
\begin{aligned}
-E_y^{inc}(\rho_n) = -\eta_s(\rho_n) I_n - j\omega\mu \sum_{m=1}^{N} I_m \int_{\Delta z} G(\rho_n, \rho_m) d\rho' \\
+ \sum_{m=1}^{N} I_m \int_{\Delta z} \eta_s(\rho_m) \frac{\partial}{\partial n'} G(\rho_n, \rho_m) d\rho'
\end{aligned}
\qquad \textbf{(3.37)}
$$

where ρ_n denotes the observation point located on the center of the nth segment on the terrain surface and ρ_m the source point of the *m*th.

The entries of the MoM impedance matrix for TM case is derived as in the same way as in equations (3.21) and (3.22),

$$
Z_{nm} = \int_{\Delta z} \left[j\omega\mu G(\rho_n, \rho_m) + \eta_m \frac{\partial}{\partial n_m} G(\rho_n, \rho_m) \right] d\rho' \qquad \textbf{(3.38)}
$$

Assuming that segments are small compared to the wave-length, about λ/10, the elements of the impedance matrix may be approximated as,

$$
Z_{nm} \cong -\frac{\omega\mu}{4} \Delta z H_0^{(2)}(k|\rho_n - \rho_m|) - j\frac{k\eta_m}{4} \Delta z H_1^{(2)}(k|\rho_n - \rho_m|)\hat{n}_m . \hat{\rho}_{nm} \qquad \textbf{(3.39)}
$$

3.2.3 Modeling of Impedance Boundary

Although the perfectly conducting ground model is adequate for many surface wave propagation, for correct modeling of reflection effects for modeling of propagation over rough applications, it is not universally applicable. A more accurate model is required for surface. Leontovich boundary condition

$$
\hat{n} \times \vec{E} = \eta_s \hat{n} \times (\hat{n} \times \vec{H}) \qquad \text{(on earth's surface)} \qquad \textbf{(3.40)}
$$

where $\hat{n}$ is the outward unit vector normal to the surface, is used to obtain surface impedance η_s ,which is derived as

$$
\eta_s = Z_0 \left[\frac{j\omega\varepsilon_0}{\sigma_g + j\omega\varepsilon_g} \right]^{1/2} \left[1 + \frac{j\omega\varepsilon_0}{\sigma_g + j\omega\varepsilon_g} \right]^{1/2} \qquad \textbf{(3.41)}
$$

for grazing angle. Here $Z_0=120\pi$ is the free-space wave impedance, ε_g and σ_g are the permittivity and conductivity of the ground, respectively.

3.2.4 PropMoM Algorithm

In Figure 3.2 PropMoM algorithm is given. As seen from the steps of flowchart terrain function is obtained from given terrain points and induced surface currents are obtained via Forward-Backward method. The scattered and incident field at the required range and height points is calculated. Besides, induced currents on the surface are calculated. Total field is obtained as the sum of incident and scattered field on the surface until the last range is reached. Propagation factor as $|E/E_0|$ and $|H/H_0|$ vs. range or height is plotted for horizontal and vertical polarizations, respectively.

Based on the algorithm below, calculations are made using MATLAB. The frequency [MHz], maximum range [m], transmitter range and height [m] are input parameters. Both range and height variations of $|E/E_0|$ and $|H/H_0|$ can be observed for horizontal and vertical polarization, respectively. Observation height and number of height points should be chosen for height variations while for range variations, an observation height above the terrain should be given. The relative permittivity [H/m], permeability [F/m] and conductivity [S/m] should be considered for non-PEC surfaces since these parameters change surface impedance.

3.2.5 Applications of PropMoM Algorithm

In this section, numerical comparisons will be given to validate MoM, with the help of calculations via MoM and 2-ray ground reflection model.

In Figure 3.3, propagation factor variation over range on a 60λ flat PEC surface can be observed in case of vertical polarization. Operating frequency is 300 MHz. For all of the figures in this section, solid line refers to MoM while dashed line refers to 2-ray ground reflection model. In the figures, observation height is 5m and transmitter is an isotropic radiator located at the origin with a height of 30m. In Figure 3.4, same terrain is assumed as an ocean-like surface. Relative permittivity and conductivity are assumed to 75 and 10^{-3}, respectively. And in Figure 3.5, terrain is assumed as an earth-like terrain. Obtained results show that MoM gives accurate results compared to 2-ray ground reflection model.

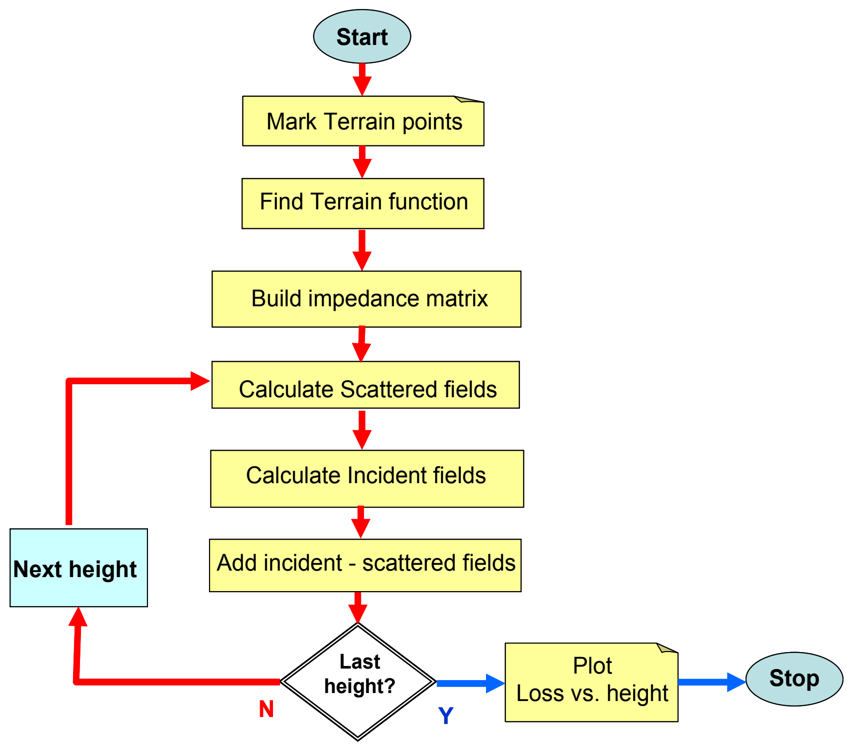

Figure 3.2: Flowchart for MoM based PropMoM Algorithm

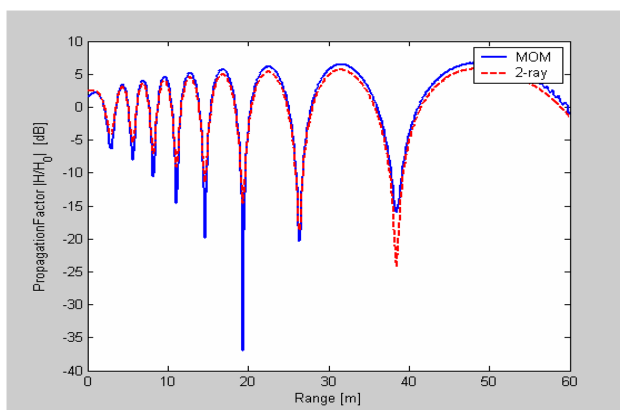

Figure 3.3 Propagation factor vs range on a 60λ flat PEC surface for vertical polarization (Transmitter height is 30m and observation height is 5m)

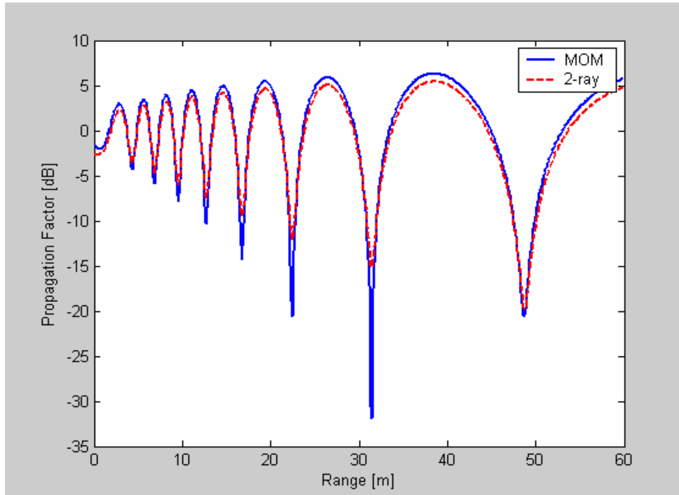

Figure 3.4 Propagation factor vs range on a 60λ flat non-PEC surface for vertical polarization (ε_r = 75, σ=0,001 are the parameters for the ocean-like surface and transmitter height is 30m while observation height is 5m)

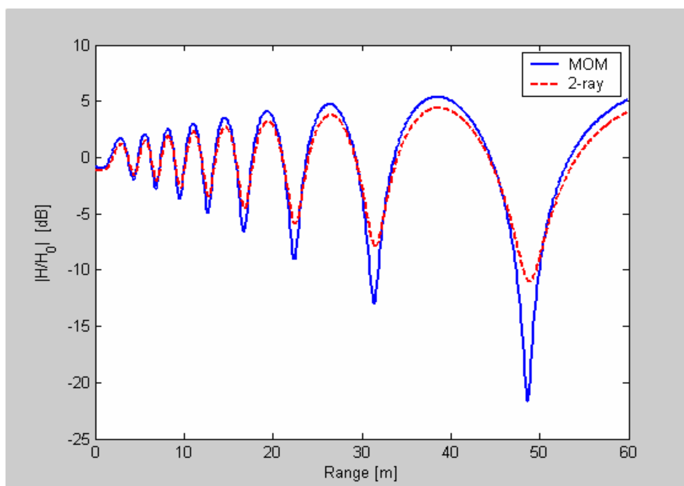

Figure 3.5 Propagation factor vs range on a 60λ flat non-PEC surface for vertical polarization (ε_r = 5, σ=10^{-3} are the parameters for the earth-like surface and transmitter height is 30m while observation height is 5m)

In Figure 3.6 propagation factor variation over range can be observed for 20λ flat PEC surface. Frequency is 300 MHz and the source is an isotropic radiator placed at 10m. The observation height for range variation is taken as 5m. In Figure 3.7 propagation factor over height variation is plotted. Observation range for the height profile is the maximum range.

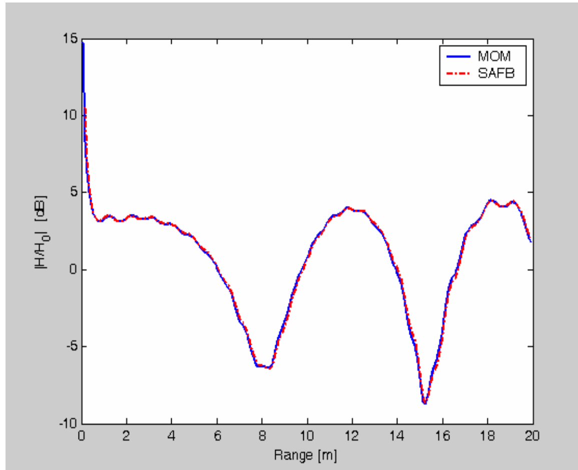

Figure 3.6 Propagation factor over range variation on a 20 λ flat PEC surface in case of vertical polarization

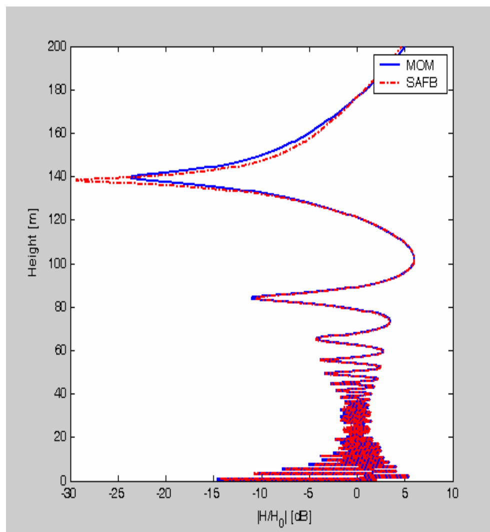

Figure 3.7 Propagation factor over height variation on a 20 λ flat PEC surface in case of vertical polarization

3.3 Forward-Backward Method (FBM)

The Forward-Backward Method (FBM) is a stationary iterative technique for solving linear system of equations resulting from electromagnetic rough surface scattering problems, causing a computational cost and a memory requirement of $O(N^2)$, where N is the number of surface unknowns.

After the discretization process as shown in Figure 3.8, integral equation is transformed into a matrix equation

$$V = \overline{Z} \cdot I \tag{3.42}$$

and [I] is the unknown current coefficients to be found.

To develop forward-backward approach, it is desirable to make the following decompositions,

$$I = I^f + I^b \tag{3.43}$$

$$\overline{Z} = \overline{Z}^f + \overline{Z}^s + \overline{Z}^b \tag{3.44}$$

where I^f is the contribution due to the wave propagation in the forward direction and I^b is the contribution due to the wave propagation in the backward direction. In equation (3.43) $\overline{Z}^f$, $\overline{Z}^s$ and $\overline{Z}^b$ are, the lower triangular part, the diagonal part (self impedance terms), and the upper triangular part of $\overline{Z}$, respectively.

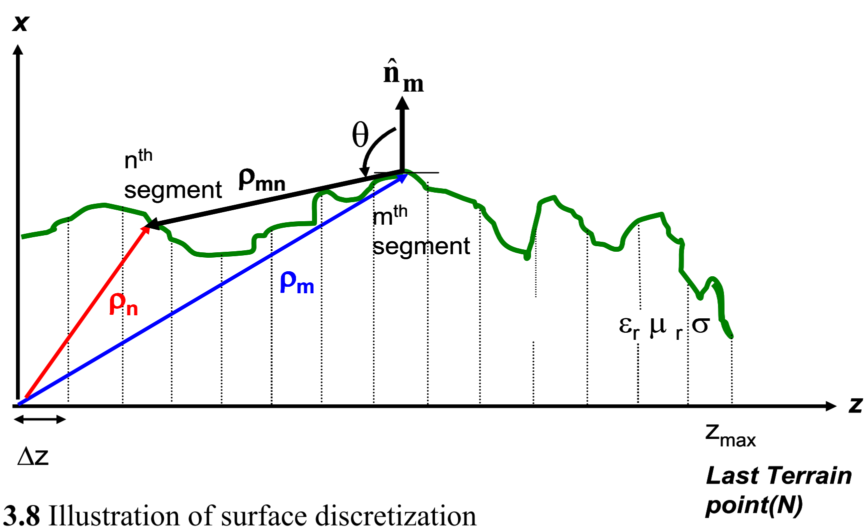

Figure 3.8 Illustration of surface discretization

Using equations (3.43) and (3.44), equation (3.42) can now be split into forward-propagation and backward-propagation matrix equations, respectively, as follows:

$$\overline{Z}^s \cdot I^f = V - \overline{Z}^f \cdot \left(I^f + I^b\right) \tag{3.45}$$

$$\overline{Z}^s \cdot I^b = -\overline{Z}^f \cdot \left(I^f + I^b\right) \tag{3.46}$$

Considering the nth element (called the receiving element) on the surface, the second term on the right-hand side of (3.45) represents the forward propagating field contribution due to the radiation of current elements preceding of receiving element, (elements where $z < z_n$), which corresponds to the nth forward region in Figure 3.1. Similarly, the term on the right-hand side of (3.46) represents the backward propagating field contribution due to the radiation of current elements following (elements where $z > z_n$) of the receiving element, so it represents the nth backward region contribution as in Figure 3.9. Therefore, (3.45) and (3.46) has been assumed by definition to describe the forward propagation and backward propagation, respectively.

The total current on the *n*th receiving element is composed of the forward and backward field-induced currents. Equations (3.45) and (3.46) can be solved iteratively, where currents in the *i*th stage of the algorithm $\left(I^{f,(i)}, I^{b,(i)}\right)$ are obtained as,

$$\left(\overline{Z}^{s} + \overline{Z}^{f}\right) \cdot \overline{I}^{f,(i)} = V - \overline{Z}^{f} \cdot I^{b,(i-1)} \quad \textbf{(3.47)}$$

$$\left(\overline{Z}^{s} + \overline{Z}^{b}\right) \cdot I^{b,(i)} = -\overline{Z}^{b} \cdot I^{f,(i)} \quad \textbf{(3.48)}$$

The algorithm starts with initializing $I^{b,0} = 0$. The matrices involved in this iterative process do not need to be factorized or inverted because $\overline{Z}^{s} + \overline{Z}^{f}$ is a lower triangular matrix, and is $\overline{Z}^{s} + \overline{Z}^{b}$ is an upper triangular matrix, so (3.47) and (3.48) can be solved for $I^{f,(i)}$ and $I^{b,(i)}$ by forward and backward substitution, respectively. Iterations are continued until surface currents show convergence to within a specified accuracy criterion. The convergence has been shown to be extremely rapid for moderately rough surfaces, generally requiring fewer than ten iterations.

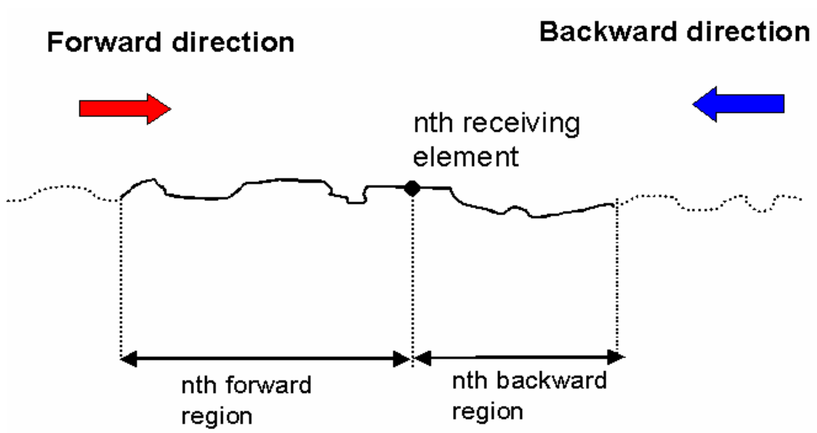

Figure 3.9 Forward and backward regions for the nth matching point.

A direct computation of the matrix multiplies in (3.47) and (3.48) produces an $O(N^2)$ algorithm, since the coupling between all pairs of points on the surface must be evaluated. Furthermore, the impedance matrix $\overline{Z}$ must be either stored at a cost of memory storage or recomputed at each iteration with a time-consuming computation. These costs typically prohibit the application of this procedure to large-scale of scattering problems such as scattering from ocean-like surfaces at near-grazing incidence [16].

When the current distribution over the terrain surface is obtained, scattered field at an observation point may be computed for vertical polarization as,

$$H_y^{scat}(\rho_n) \cong \frac{\Delta z \omega \varepsilon}{4} \sum_{m=1}^{N} I_m \eta_m H_0^{(2)}(k|\rho_n - \rho_m|) + j \frac{k\Delta z}{4} \sum_{m=1}^{N} I_m H_1^{(2)}(k|\rho_n - \rho_m|) \hat{n}_m . \hat{\rho}_{nm} \qquad \textbf{(3.49)}$$

and for horizontal polarization as,

$$E_y^{scat}(\rho_n) \cong -\frac{\Delta z \omega \mu}{4} \sum_{m=1}^{N} I_m H_0^{(2)}(k|\rho_n - \rho_m|) + j\Delta z \frac{k}{4} \sum_{m=1}^{N} I_m \eta_m H_1^{(2)}(k|\rho_n - \rho_m|) \hat{n}_m . \hat{\rho}_{nm} \qquad \textbf{(3.50)}$$

Total field is calculated as sum of incident and scattered fields by,

$$H_y^{tot} = H_y^{scat} + H_y^{inc} \qquad \textbf{(3.51)}$$

for vertical polarization and

$$E_y^{tot} = E_y^{scat} + E_y^{inc} \qquad \textbf{(3.52)}$$

for horizontal polarization.

The FBM may not exhibit convergent behavior for surfaces where the Method of Moment (MoM) current elements are not numbered sequentially as a function of increasing z coordinate such as a ship or a large breaking wave on the ocean surface. The Generalized Forward-Backward Method (GFBM), which is a hybrid method based on a combination of the conventional FBM with MoM, was proposed to overcome this limitation.

3.4 Spectrally Accelerated Forward – Backward Method

A direct computation of the matrix multiplies in (3.47) and (3.48) produces an *O(N^2)* algorithm since the coupling between all pairs of points on the surface must be evaluated. Furthermore, the impedance matrix Z must be either stored at a cost of *O(N^2)* memory storage or recomputed at each iteration with a time-consuming computation. These costs typically prohibit the application of this procedure to large-scale scattering problems such as scattering from ocean-like surfaces at near-grazing incidence.

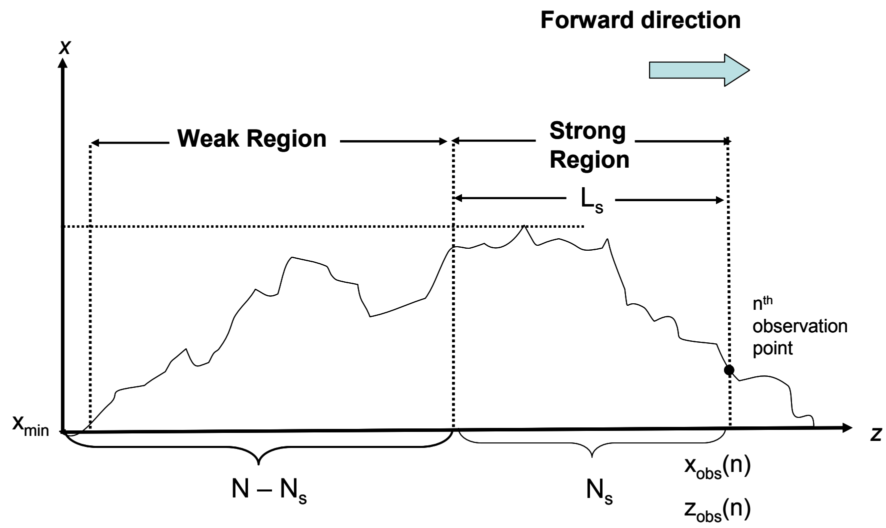

Figure 3.10 Selection of strong region distance and elements

The iterative forward-backward procedure described in sections 3.1.1 and 3.1.2 requires repeated computation of the matrix-vector products,

$$E_f(\rho_n) \cong \sum_{m=1}^{n-1} I_m Z_{nm} \tag{3.53}$$

$$E_b(\rho_n) \cong \sum_{m=n+1}^{N} I_m Z_{nm} \tag{3.54}$$

for horizontal polarization, which denote the forward and backward radiations by source current elements preceding and following for the receiving nth element, respectively. Here $O(N^2)$ operational count is required.

The acceleration algorithm starts with the decomposition of E_f in terms of strong interaction contribution E^s and weak interaction contribution E^w, respectively. E^s is the field radiated from the strong interaction source group, which is selected within neighborhood distance L_s of receiving n^{th} element. Problem geometry can be found in Figure 3.10 .It is noted that in most of the practical cases, L_s is a very small portion of the surface length and remains fairly fixed for a given roughness of surfaces regardless of the surface length, and therefore, E^s is found via the conventional exact computation. On the other hand, E^w, which is radiated from the source group selected outside the strong interaction source group, becomes important when the angle of wave incidence is near grazing or if one is interested in backscattered field.

As a result, (3.53) and (3.54) can be written as

$$E_f(\rho_n) \cong \sum_{m=N-N_s}^{n-1} I_m Z_{nm} + \sum_{m=1}^{n-N_s-1} I_m Z_{nm} \tag{3.55a}$$

$$E_f(\rho_n) \cong E_f^s(\rho_n) + E_f^w(\rho_n) \tag{3.55b}$$

and

$$E_b(\rho_n) \cong \sum_{m=n+N_s}^{n+1} I_m Z_{nm} + \sum_{m=N}^{n+N_s+1} I_m Z_{nm} \tag{3.56a}$$

$$E_b(\rho_n) \cong E_b^s(\rho_n) + E_b^w(\rho_n) \tag{3.56b}$$

respectively where $N_s=L_s/\Delta z$ denotes the number of elements that have strong interactions with the n^{th} element. The first terms in (3.55b) and (3.56b) denoted by E^s represent the strong region contributions and the second terms denoted by E^w represent the weak region contributions. E^s is found in a conventional manner using the exact matrix elements of diagonal as described in sections (3.1.1) and (3.1.2).

Rapid computation of E_w is performed by employing the spectral acceleration of Hankel function $H_0^{(2)}$

$$H_0^{(2)}(k|\rho_n - \rho_m|) = \frac{1}{\pi} \int_{C_\phi} e^{jk[(z_n - z_m)\cos\phi + (x_n - x_m)\sin\phi]} d\phi \tag{3.57}$$

where C_ϕ is the contour of integration in the complex ϕ space shown in Figure 3.4.

In vertical polarization, forward and backward procedure equations are obtained respectively as,

$$H_f(\rho_n) \cong \sum_{m=1}^{n-1} I_m Z_{nm} \tag{3.58}$$

$$H_b(\rho_n) \cong \sum_{m=n+1}^{N} I_m Z_{nm} \tag{3.59}$$

The neighborhood distance L_s is chosen and within interactions between points are classified as strong and outside of which interactions are classified as weak, to apply spectral acceleration. As a result, (3.58) and (3.59) can be written as

$$H_f(\rho_n) \cong \sum_{m=N-N_s}^{n-1} I_m Z_{nm} + \sum_{m=1}^{n-N_s-1} I_m Z_{nm} \tag{3.60a}$$

$$H_f(\rho_n) \cong H_f^s(\rho_n) + H_f^w(\rho_n) \tag{3.60b}$$

and

$$H_b(\rho_n) \cong \sum_{m=n+N_s}^{n+1} I_m Z_{nm} + \sum_{m=N}^{n+N_s+1} I_m Z_{nm} \tag{3.61a}$$

$$H_b(\rho_n) \cong H_b^s(\rho_n) + H_b^w(\rho_n) \tag{3.60b}$$

3.4.1 Deformed Contour of Integration

Since the Hankel function is analytic in this plane for widely separated points, the contour of integration can be deformed to a steepest path (SDP). For example, for a flat surface such than x_n-$x_m=0$, the SDP path obtained is as shown in Figure 3.11, and an asymptotic analysis demonstrates that most of the contribution occurs on portions of the SDP near a saddle point on the real axis. As the distance from the saddle point increases along the SDP, complex values of ϕ on the SDP result in exponential attenuation of the integrand of equation (3.57) so that the contributions become negligible. This deformation of the interaction contour can be very advantageous numerically, since the contributing region of the path is usually much smaller than the original integration path C_ϕ, resulting in a smaller integration interval required. In addition, rapid oscillations of the integrand can be reduced allowing a smaller sampling rate in calculating the integral. A SDP can be similarly found for pairs of points with z_m-$z_n \neq 0$, with the saddle point located at

$$\phi_s = \tan^{-1}\left(\frac{x_n - x_m}{z_n - z_m}\right) \tag{3.61}$$

on the real axis. This angle for ϕ_s represents the direct ray connecting the source and receiving elements, demonstrating that the most significant contribution arises from the lit region of the source element.

If groups of source and receiving elements are considered, the effect is to introduce several saddle points onto the real axis, located at real values of phi given by ϕ_s above for each pair of elements making up the groups. The width along the real axis to which these saddle points extend will be defined as the asymptotic lit region in the spatial domain, as shown in Figure 3.11, which is analogous to the geometrical optics (GO) region defined in theory of diffraction [UTD] [17].

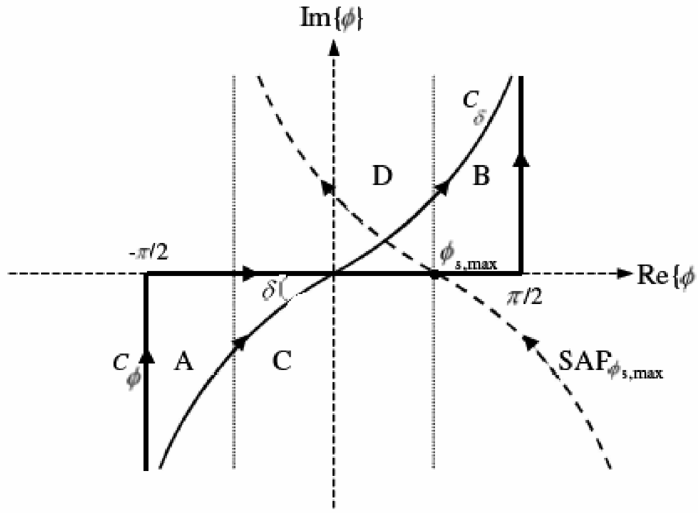

Figure 3.11 Integrand of contour of $H_0^{(2)}$ on the complex phi plane

Parts of the real axis outside the lit region are classified as the asymptotic shadow region in the space domain. Therefore, C and D can be defined as the lit region in the spatial domain, while A and B are defined as the shadow regions in Figure 3.11.

Since contributions between several source and receiving elements on the surface are now being considered simultaneously, there is no longer a unique SDP along which only the attenuation of the integrand is obtained away from a single saddle point. It can still be shown that the portions of all paths in regions A and B provide only small contributions to the integral due to either exponential attenuation or fast oscillation of the integrand. The portions of paths in regions C and D in Figure 3.11, however, now mix both descent and ascent paths where the integrand $F_n(\phi)$ may exponentially increase, particularly for large z deviations, i.e. rougher surfaces, where the lit region becomes larger.

To avoid numerical difficulties in the integration caused by this exponential growth, it is desirable (a) to choose L_s that yields a small spatial domain lit region, and (b) to deform the contour of integration from C_ϕ to C_δ which is a path between C_ϕ and the SDP for a flat surface as shown in Figure 3.11. C_ϕ is defined to be a straight line with slope tan δ through regions C and D. It is noted that δ = π/4 for a flat surface, but this angle is chosen to be smaller for more rough surfaces in order to avoid extreme exponential growth rates in regions C and D. Outside the lit region, C_δ is deformed into the deep shadow regions so that shadow region contributions are insignificant.

One criterion for selecting δ can be obtained by limiting the maximum value of the integrand on the path to e^2 [16]. The equation which results specifies $\delta = \tan^{-1}(1/b)$, with

$$b = \max\left[\sqrt{\frac{kR_s}{20}}\phi_{s,\max} - 1, 1\right] \quad \textbf{(3.62)}$$

which insures that the SDP of a flat surface path is obtained for at surfaces but a smaller value of δ is used as the surface becomes more rough. In (3.62),

$$R_s = \sqrt{L_s^2 + \left(x_{\max} - x_{\min}\right)^2} \quad \textbf{(3.63)}$$

and

$$\phi_{s,\max} = \tan^{-1}\left(\frac{\left(x_{\max} - x_{\min}\right)}{R_s}\right) \quad \textbf{(3.64)}$$

are used since it is the saddle point at the shadow boundary with the largest distance between source and observation points that produces the largest possible value of the integrand. This choice of δ also insures that along C_δ the plane waves of the integrand in equation (3.29) will attenuate outside the lit region as expected.

Substituting (3.57) into (3.56a) and interchanging the integration and summation gives

$$E_w(\bar{\rho}_n) = -\frac{\omega\mu}{4\pi}\int_{C_\delta} F_n(\phi)d\phi \quad \textbf{(3.65)}$$

where

$$F_n(\phi) = \sum_{m=1}^{n-N_s-1} I_m e^{jk\left[(z_n - z_m)\cos\phi + (x_n - x_m)\sin\phi\right]} \quad \textbf{(3.66)}$$

in horizontal polarization which is similar to a spectral domain FMM procedure [18], showing that weak element contributions at point ρ_n can be obtained through a spectral domain integral of the weak element complex far-field pattern or plane wave spectrum, $F_n(\phi)$.

In the same way, by substituting (3.57) into (3.56a) and interchanging the integration and summation, equation (3.65) is obtained for backward sweep where

$$F_n(\phi) = \sum_{m=N}^{n+N_s+1} I_m e^{jk[(z_n - z_m)\cos\phi + (x_n - x_m)\sin\phi]} \tag{3.67}$$

However instead of splitting the surface into several segments as done in [19], the algorithm considers only one weak interaction group made up of all source elements outside the strong region preceding (for forward computations) or following (for backward computations) the receiving element.

$F_n(\phi)$ is calculated easily from weak element currents through a recursive procedure by,

$$\begin{aligned} \mathrm{F_n}(\phi) = {} & \mathrm{F_{n-1}}(\phi)\mathrm{e}^{\mathrm{jk}[(\mathrm{z_n}-\mathrm{z_{m-1}})\cos\phi + (\mathrm{x_n}-\mathrm{x_{m-1}})\sin\phi]} + \mathrm{I_{n-1-N_s}} \\ & \Delta\mathrm{z}\left\{1 - \frac{\eta_\mathrm{s}}{\eta_0}\left[\cos\theta_{\mathrm{n-1-N_s}}\cos\phi + \sin\theta_{\mathrm{n-1-N_s}}\sin\phi\right]\right\}\mathrm{e}^{\mathrm{jk}[(\mathrm{z_n}-\mathrm{z_m})\cos\phi + (\mathrm{x_n}-\mathrm{x_m})\sin\phi]} \end{aligned} \tag{3.68}$$

with $F_n(\phi) = 0$ for $n \leq Ns + 1$ in the forward sweep. Note that $F_n(\phi)$ is independent of the receiving element except for a shift in reference point to z_n in order to avoid numerical error. Equation (3.68) shows that $F_n(\phi)$ continuously updates as each new source element enters the weak interaction group in the forward sweep.

The integral of (3.65) over ϕ can be discretized into $2Q + 1$ plane wave directions and mapped onto the real axis according to

$$d\phi \quad \to \quad \Delta\phi e^{-j\delta} \tag{3.69}$$

$$\phi \quad \to \quad \phi_p = p\Delta\phi e^{-j\delta} \tag{3.70}$$

and Q can be found from

$$Q = \left\lceil \frac{2\phi_{s,\max}}{\Delta\phi} \right\rceil \tag{3.71}$$

where $\lceil . \rceil$ denotes the nearest integer larger than the argument. Tests for several rough surfaces have shown that a value of

$$L_s \geq \frac{(x_{\max} - x_{\min})}{4} \tag{3.72}$$

approximation can yield accurate results [20]. These selections were obtained from numerical studies of the attenuation of the integrand (3.57) along the SDP of a flat surface and may not hold for very rough surfaces.

An equation for $\Delta\phi$ was developed through a study of far field patterns of a uniform current distribution on an L-L_s long flat surface and showed that approximately 44 samples are required in the main lobe region of a at surface pattern, i.e.

$$\Delta\phi = \sqrt{\frac{5}{kR_s}} / 22 \tag{3.73}$$

3.4.2 PropSAFB Algorithm

Calculations are made via FORTRAN for this technique. In order to solve large dimensional matrices, FORTRAN is used for SAFB algorithm. This program computes scattered field and total field. Propagation factor is obtained by taking the ratio of total field and incident field. In height variation of the field is calculated at maximum range while range variation is computed for a chosen height.

Input parameters for PropSAFB algorithm are given in Table 3.1. Operating frequency [MHz] is used to determine wave length and range step size (Δz) is directly chosen. Usually, taking λ/10 segmentation gives accurate results, but in this work Δz is taken as λ/5 because of computer capability and memory limitations. The results obtained by assuming step size as λ/5 segmentation are obtained to be quite satisfactory. Maximum range is assumed in [km] from origin. Permittivity and conductivity of terrain is used for defining surface impedance. Transmitter parameters are given as range and height in [m] and observation height is chosen above the terrain in [m]. Different types of transmitters can be selected as; isotropic radiator, plane wave source, infinitesimal dipole and line source in spectral representation. If transmitter is selected as plane wave, two different cases can be considered as grazing incidence and normal incidence where incidence angles are taken as π/20 and π/2, respectively. Both vertical and horizontal polarization effects can be observed. In illustrations, propagation factor is defined as $|F| = |(E_{scat} + E_{inc})/E_{inc}|$ for horizontal polarization and $|F| = |(H_{scat} + H_{inc})/H_{inc}|$ for vertical polarization. Here incident field corresponds to the free space propagation, therefore propagation factor is used to analyze the effects of propagation medium.

Table 3.1 Command panel for PropSAFB FORTRAN code

```
FREKANS [MHz] = ?
5
MAXIMUM RANGE [km] = ?
30
PERMITIVITY OF TERRAIN [eps] = ?
7
CONDUCTIVITY OF TERRAIN [sigma] = ?
.001
TRANSMITTER RANGE [m] = ?
0
TRANSMITTER HEIGHT [m] = ?
30
OBSERVATION HEIGHT [m] = ?
9.77
TYPE OF THE TRANSMITTER = ?
1-ISOTROPIC RADIATOR
2-PLANE WAVE RADIATOR
3-INFINITESIMAL DIPOLE RADIATOR
4-LINE SOURCE
5-GAUSSIAN PATTERN
4
1-NORMAL INCIDENCE (TETA=PI) = ?
2-GRAZING INCIDENCE (TETA=PI/2) = ?
2
POLARIZATION TYPE = ?
1-HORIZONTAL [TM]
2-VERTICAL [TE]
2
RE(surf_imp),IM(surf_imp)=     (3.290793E-01,-6.826710E-02)
```

3.4.3 Numerical Applications

The results obtained via SAFB method over irregular terrain are compared to the results obtained via SSPE, in order to validate the method. Observation points are assumed to be located at a given height above terrain. In SSPE, for vertical and horizontal polarization Neumann boundary and Dirichlet boundary conditions are used for PEC ground, respectively. Computational height for SSPE solution is assumed as 40 km and FFT size for height profile is assumed as 4096. Choosing maximum height less than 40 km causes unwanted and nonphysical reflections from the top boundary become dominant. For PEC terrain profiles, surface impedance is considered as zero in SAFBM.

The source types used in SAFB and SSPE can be different for the computation of propagation factor. In SSPE, the initial field is given as a Gaussian source vertically in spatial domain. However, the comparison in terms of the magnitude of the field requires the same sources in both SSPE and SAFB method. In order to achieve this, line source is used in SAFB method and height variation of initial field, which is required by SSPE is produced inside SAFB algorithm at the transmitter range. Then this initial field obtained via SAFB method is applied in SSPE. This produces guarantee of the equality of incident fields because SSPE solution corresponds to cylindrical propagation.

From the calculations, it is observed that, after six or seven iterations, the values converge to an accuracy level of small error.

In Figure 3.12, propagation factor vs range for a flat terrain is illustrated. Operating frequency is 5 MHz. In the figure, dotted line shows split-step parabolic equation (SSPE) solution while solid line is the graph of spectrally accelerated forward-backward method (SAFB). Observation height is 21.97 m and transmitter is placed at 100 m. while source is a line source. In Figure 3.13 magnitude of total field variation over range is illustrated with same parameters.

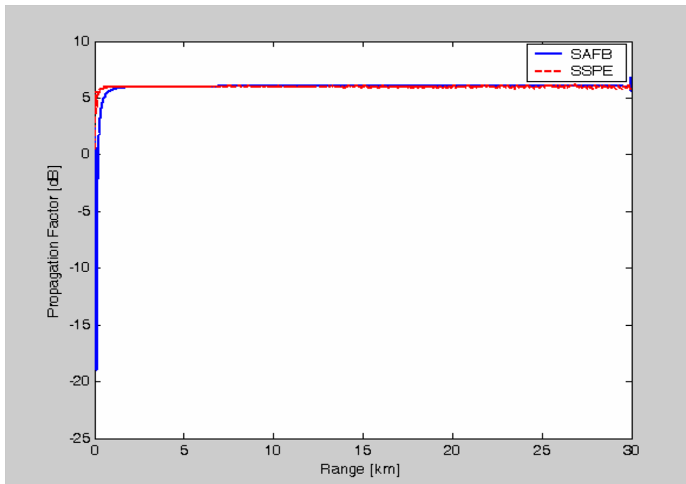

Figure 3.12 Propagation factor over range variation on a 500λ flat PEC surface in case of vertical polarization observed at 9.76m height above flat terrain with a line source at 30m height

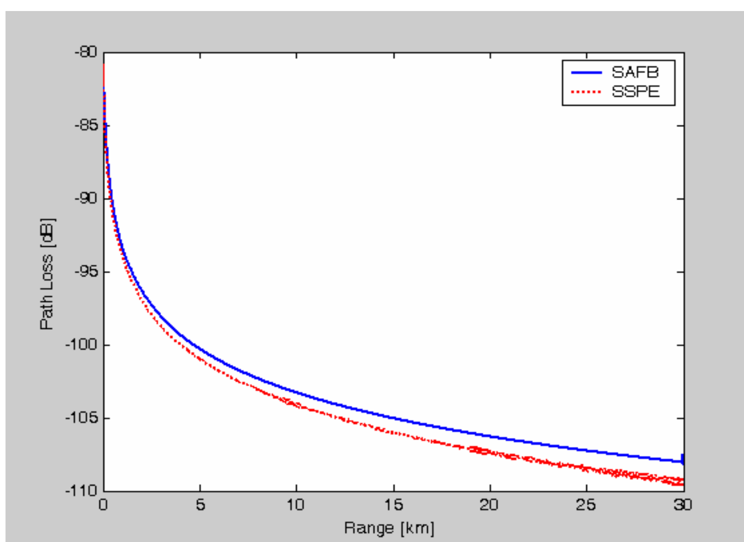

Figure 3.13 Magnitude of total field vs. range in vertical polarization at 9.76m observation height with line source at 100m height for a flat PEC terrain

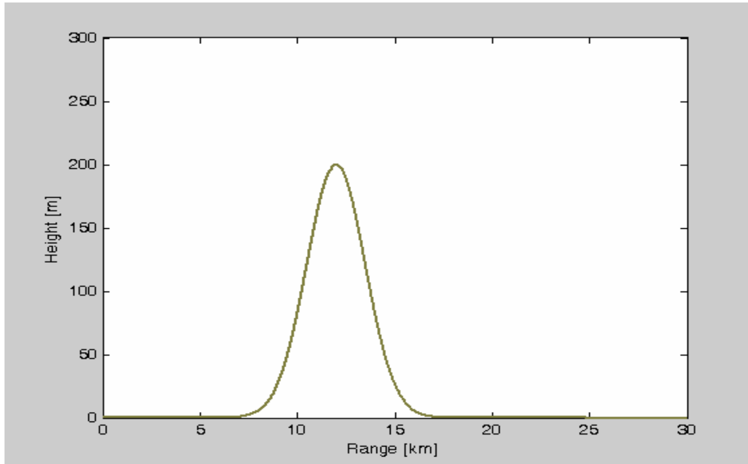

Figure 3.14 Terrain profile: A gaussian hill with 200 m height

In Figure 3.15, propagation factor variation vs range obtained for the terrain profile shown in Figure 3.14 is plotted. Solid line corrresponds to the results calculated via SAFB and dash-dot line corrresponds to the results calculated via SSPE, respectively. In this geometry transmitter is a line source located at 100 m height at the origin and the operating frequency is chosen as 5 MHz. Observation points are assumed as 21.97m height above terrain. This figure shows that there is a good agrrement between SAFB and SSPE.

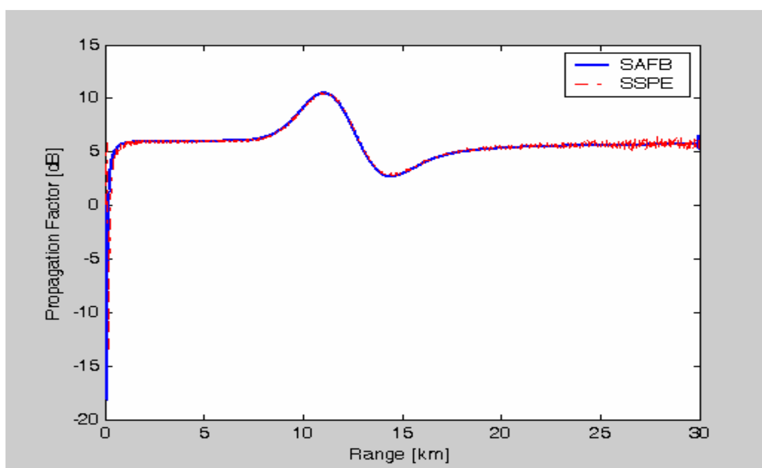

Figure 3.15 Propagation factor variation over range on a 500λ PEC Gaussian-like terrain in vertical polarization (Solid: SAFB, Dash-dot: SSPE)

In Figure 3.16, magnitude of total field variation over range is shown. In the figure, solid and dashed lines correspond to the results obtained for the same terrain profile given in Figure 3.14 via SAFB and SSPE, respectively. Dotted line corresponds to the result obtained via SAFBM solution for the flat PEC surface.

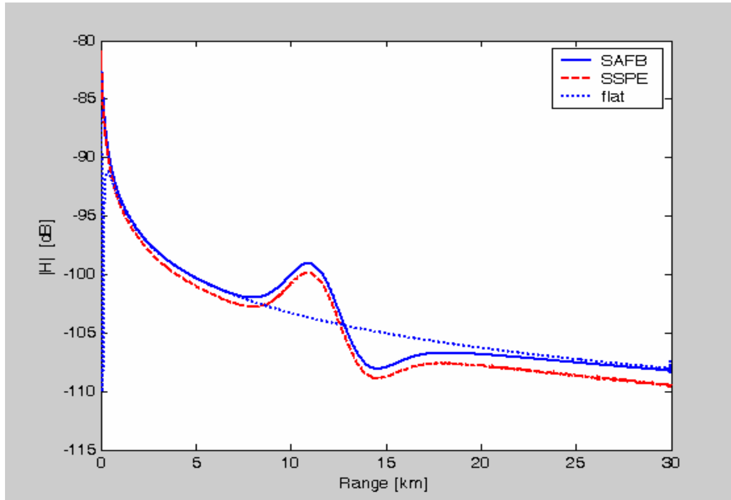

Figure 3.16 Magnitude of total field variation over range on a 500λ PEC Gaussian-like terrain for vertical polarization (Solid: SAFB, Dash: SSPE, Dot: Flat SAFB)

In Figure 3.17, a triangular terrain profile of 200 m height with its vertex is at about 12 km, is illustrated. The terrain geometry is assumed similar to Gaussian like terrain profile given in Figure 3.14. Triangular terrain has a knife-edge profile which is different from Gaussian terrain which has a convex shape.

In Figure 3.18, magnitude of the total H-field over range variation is plotted for the PEC triangular hill profile illustrated in Figure 3.17. Frequency is 5 MHz and the transmitter is located at (z=0, x=30m) in case of vertical polarization. In this figure, dashed and solid lines correspond to results obtained for propagation over terrain via SSPE and SAFB while dotted line represents the solution for propagation over flat surface, respectively.

Figure 3.19 is the illustration for a rough terrain profile in which two Gaussian-like hills are located adjacently with 140m and 180m heights.

In Figure 3.20, magnitude of total field variation over range is plotted in dB when observation height is assumed as 9.7m above from the terrain. Solid line illustrates SAFB method calculation while dashed line illustrates SSPE method and dash-dot line is the illustration for flat surface without terrain.

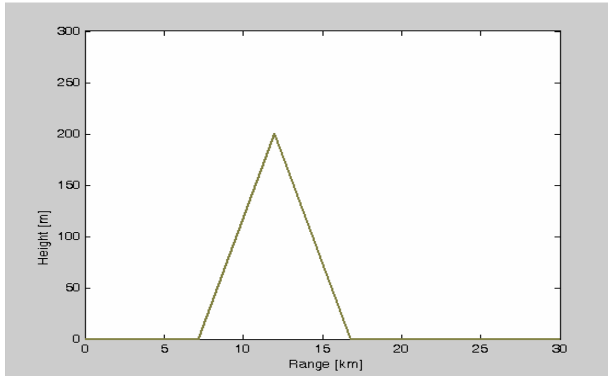

Figure 3.17 Terrain profile: A triangular hill with 200 m height vertex

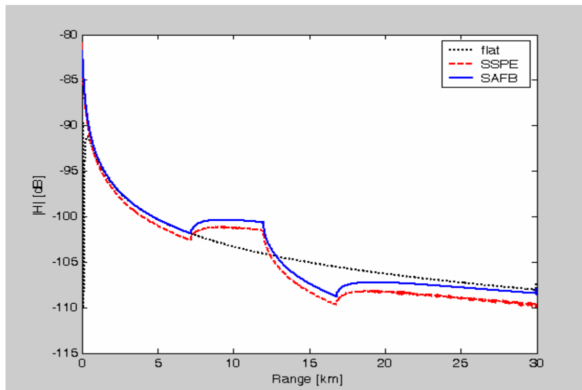

Figure 3.18 Magnitude of total field over range variation on a triangular PEC terrain in vertical polarization

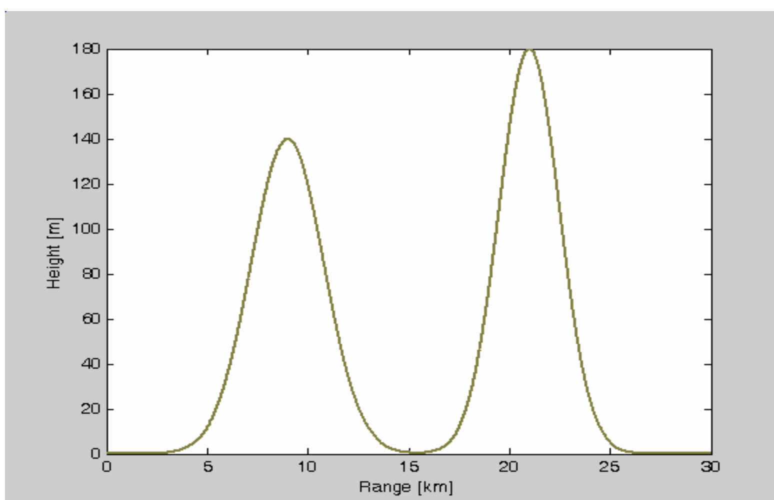

Figure 3.19 Terrain profile: Two consecutively placed Gaussian PEC hills with 140 m and 180 m heights

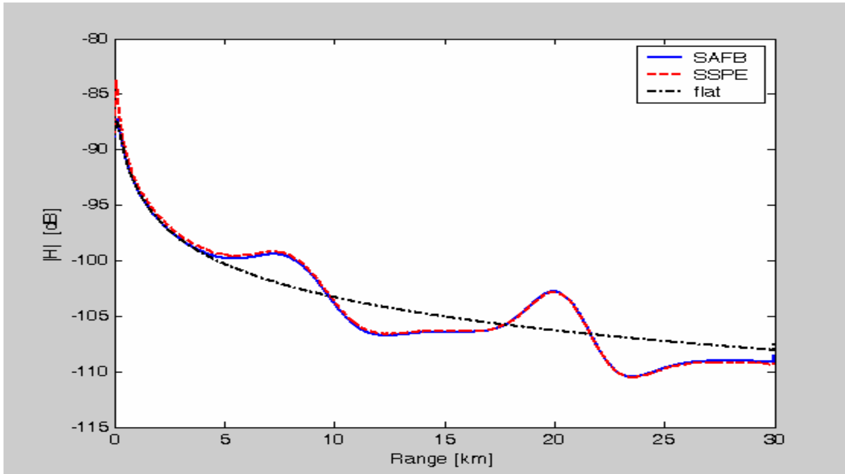

Figure 3.20 Magnitude of total field variation over range on a two-gaussian hill terrain profile in case of vertical polarization

As seen from the figures above, the ripples of the plots of total field and propagation factor are because of irregular terrain existence. A good agreement is observed between SSPE and SAFB method for different types of terrain profiles. It is seen in most of propagation scenarios that total field generally decreases behind the obstacle as expected.

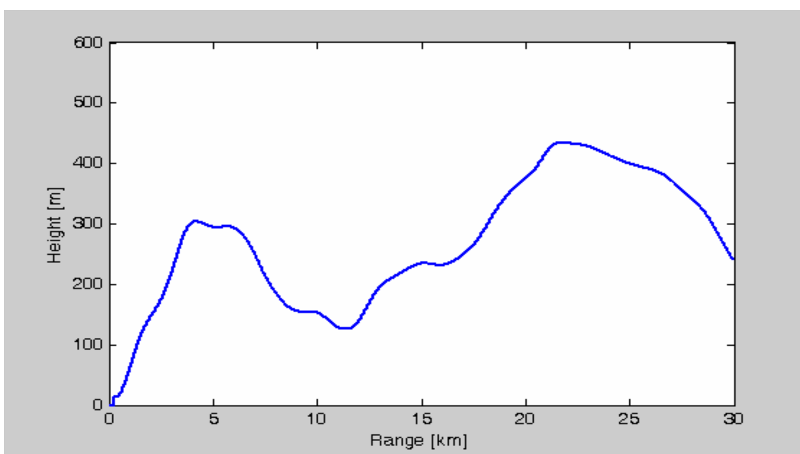

Figure 3.21 A concave-convex terrain profile of 500λ

In Figure 3.21, a rough terrain profile of maximum 30km length is seen. In Figure 3.22, propagation factor variation vs range is obtained via SAFB method, for the terrain illustrated in Figure 3.21, is plotted. Here, frequency is chosen as 10 MHz and the transmitter is considered as an isotropic radiator located at 30m high above ground. In the figure, solid line refers to the results obtained for PEC terrain while dotted line refers to the results obtained for non-PEC terrain. Non PEC terrain is assumed as ground with a relative permittivity of 5 [F/m] and conductivity of 0.01 [S/m] when the terrain is lossy, amplitude of propagation factor decreases since the energy is penetrated.

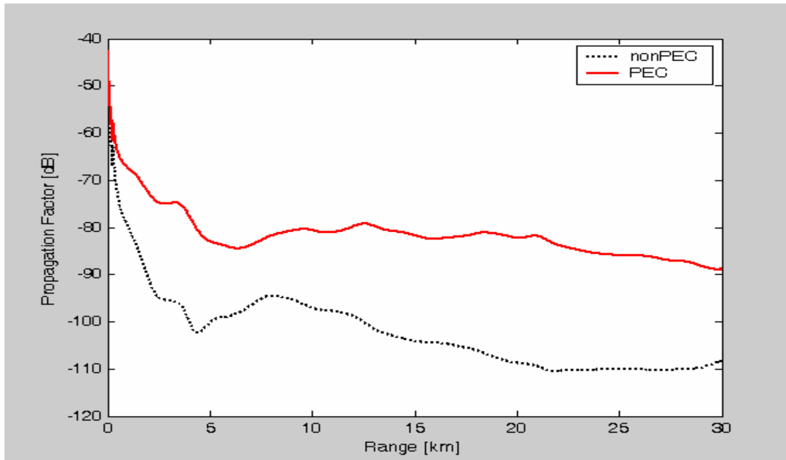

Figure 3.22 Propagation factor over range for a 500λ rough terrain in vertical polarization with different surfaces (Dot: non-PEC, Solid: PEC)

In Figure 3.23, rough terrain profiles of 15km length for two consecutively placed Gaussian terrains are illustrated. Height of first terrain is 300m while second terrain is 600m. In Figure 3.24, total field variation over range in vertical polarization at 10 MHz is plotted. Transmitter is located at 10m and observation height is 5m. In the figure, solid line refers to the results obtained for PEC terrain via SAFB method, dash line refers to the results obtained for PEC terrain via SSPE method and dash-dot refers to the results obtained for non-PEC terrain via SAFB method. It is shown that SAFB and SSPE give exact results for PEC terrain. Non PEC terrain is assumed as ground with a relative permittivity of 5 [F/m] and conductivity of 0.01 [S/m]. When the terrain is lossy, energy is penetrated, field variation decreases.

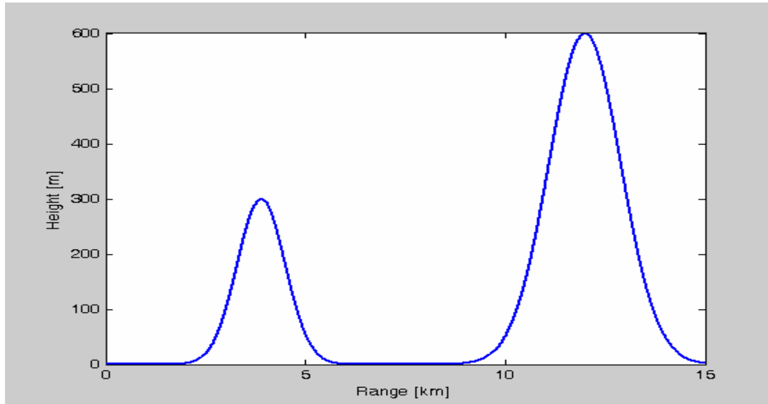

Figure 3.23 Terrain profile: Two consecutively placed Gaussian PEC hills

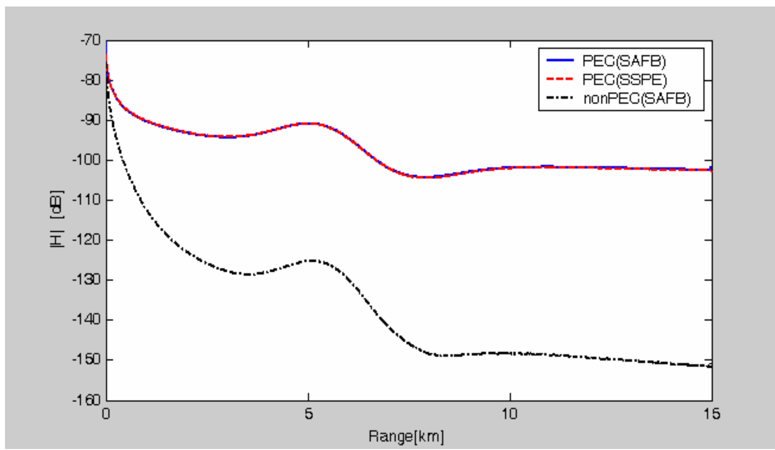

Figure 3.24 Total field variation over range for a 2-hill Gaussian terrain in vertical polarization at 10 MHz (Solid: SAFB on PEC terrain Dash: SSPE on PEC terrain Dash-dot: SAFB on non-PEC terrain)

In Figure 3.25, sea-land-sea transition where island height is taken as 300m is illustrated. Island is illustrated as a Gaussian curve while sea is illustrated as flat. Relative permittivity is taken as ε=5 [F/m] and conductivity as σ=0.01 [S/m] for land, which makes the surface impedance η_s=46.7+j41.8, and for sea surface impedance is assumed as η_s=0.

In Figure 3.26, total field variation over range of a mixed-path profile is illustrated at vertical polarization at 5 MHz. Solid line refers to the result when only the island is assumed as non-PEC while dash line refers to the result when all terrain is assumed as PEC. Transmitter is accepted to be a line source.

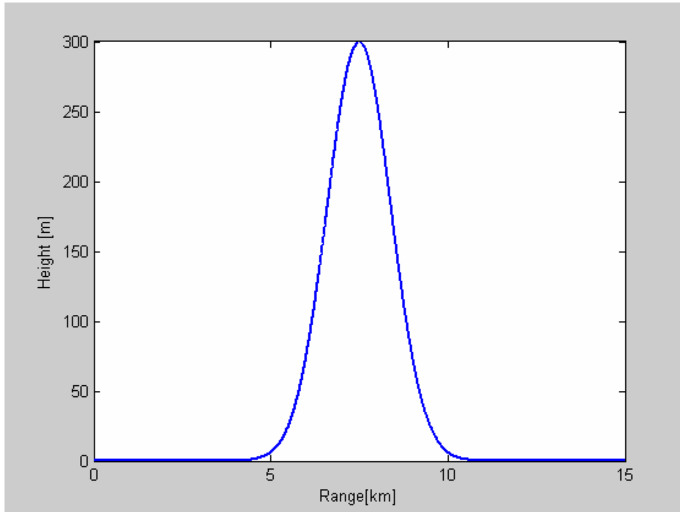

Figure 3.25 Mixed-path profile of sea-land-sea transition where island height is 300m

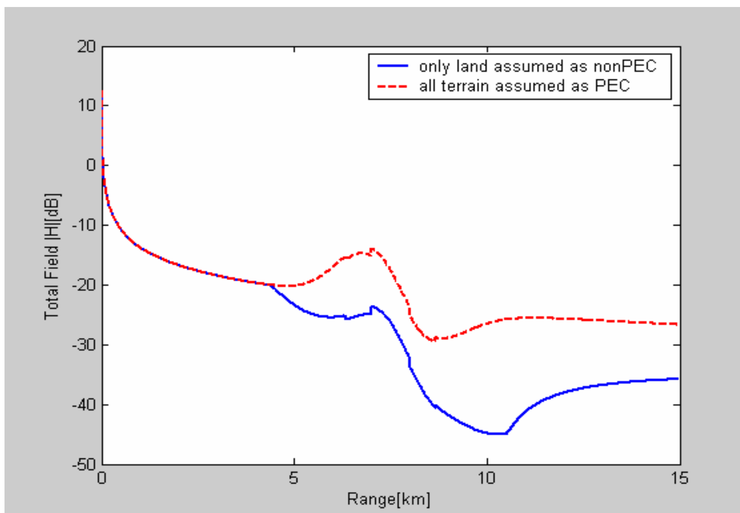

Figure 3.26 Total field variation over range for the island in vertical polarization at 5 MHz

In Figure 3.27, total field variation over range of a sea a mixed-path profile is illustrated at vertical polarization at 5 MHz. Solid line refers to the result obtained for with land assumed as non-PEC via SAFB, dashed line refers to the result obtained for without land assumed as non-PEC via SAFB.

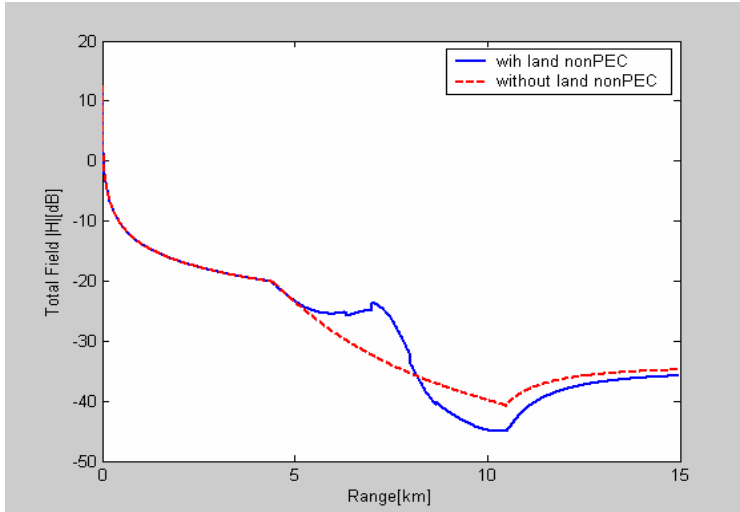

Figure 3.27 Total field variation over range for the island in vertical polarization at 5 MHz

In Figure 3.28, surface wave path loss versus range over mixed-path (island transition, a 5.2km length island 5.2km away from the source) at two different frequencies. At the left side, top is the path loss versus range obtained via SAFB at a frequency of 10 MHz; bottom is the path loss versus range obtained via SAFB at15 MHz. And at the right hand side, path loss over range is illustrated for two other methods. Solid lines refer to the result obtained via Waveprob, line with squares refer to the results obtained via TDWP (Time Domain Wave Propagator). Accuracy of TDWP and Waveprob are shown in an earlier work. Reader can find it detailly in [Chapter 2 and 4, 8].

Multi-mixed path propagation effects along ocean paths in the presence of different-length, different-height and islands including range differences between islands is an important EM propagation problem for radar technologies and long range communication. Here, the atmospheric characteristics are not considered and the electromagnetic wave is assumed to be propagating through homogeneous medium (i.e., free space). However these results show that SAFB also gives accurate results for sea-land-sea transition profiles.

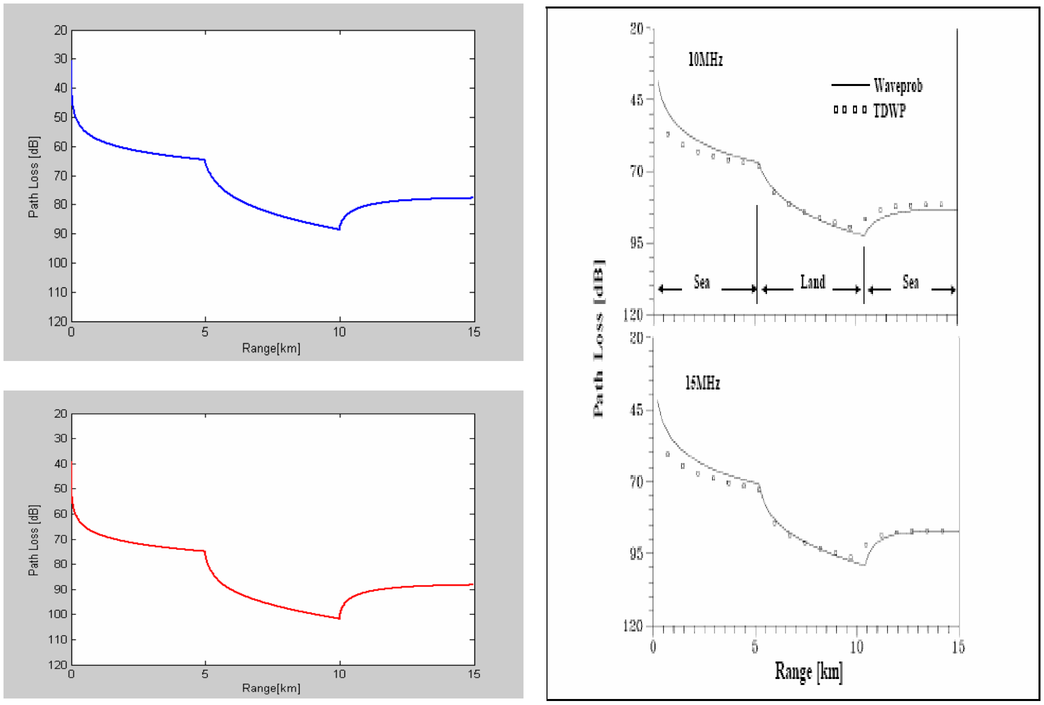

Figure 3.28 Surface wave path loss versus range over mixed-path (island transition, a 5.2km length island 5.2km away from the source) at two different frequencies. (a) Left top: Path loss calculation at 10MHz obtained via SAFB (b) Left bottom: Path loss calculation at 15MHz obtained via SAFB (c) Right top: Path loss calculation at 10MHz obtained via Waveprob and TDWP (d) Right bottom: Path loss calculation at 10MHz obtained via Waveprob and TDWP.

4. CONCLUSIONS AND DISCUSSIONS

In this thesis, the problem of ground wave propagation over non-flat, imperfect earth's surface through homogeneous atmosphere has been investigated via both MoM based Spectrally Accelerated Forward Backward Method (SAFBM) and Split Step Parabolic Equation (SSPE). These are both frequency domain methods.

The main conclusions of this work are can be stated as following:

- SSPE is efficient and reliable for modeling narrow-band wave propagation (especially for frequencies VHF and above) over weakly back-scattering rough surfaces, above which exists a vertically and/or horizontally varying refractivity profile. As SSPE is an initial value problem, once the initial profile is applied, it is longitudinally propagated through a medium defined by longitudinally as well as transversely varying refractivity over longitudinally changing non-flat profile. SSPE is an efficient engineering tool and has been in use for nearly two decades to handle forward scattering propagation problems.

- MoM is a very-well known frequency domain method for a few decades [22]. And MoM is based on the calculation of currents on small segments because of matrix-system formulation. The memory and computation time increases proportionally with the complexity of problem as the number of segments increases. The number of segments depends on the size of structure and the operating frequency. Segmentation of a length of $\lambda/10$ is usually a good approximation for most of problems. In this piece of work, our computer capability was enough for $\lambda/5$ approximation but seen from the results this was is a good approximation for maximum range. In MoM, diffraction effects are not taken into account so edge and tip treatments in problem geometries must be handled via some other methods.

- Direct solution of this matrix form results in the segment currents from which the scattered fields at any specified observation point can be calculated using the Green's function propagator. Obviously, the solution of MoM is very time consuming as the number of segments increase. Instead of the direct solution of the system of N unknowns, which requires $O(N^3)$ operations, the forward-backward spectral acceleration (FBSA) with $O(N)$ operations is used in order to find the unknown current coefficients for electrically very large terrains. It should be noted that the FBSA can take into account the variations of the electrical parameters of the surface therefore different combinations of land-sea transitions are possible. On the other hand, it can not take the refractivity variations into account, therefore only terrain effects can be investigated with this method.

- The Spectral Acceleration algorithm was proposed to overcome the computational limitation of the FBM. This technique reduces the computational cost and memory requirements to $O(N)$, so that the Spectrally Accelerated Forward-Backward Method (FBSA) can be applied over very large one-dimensional quasi-planar surfaces.

It has been shown that MoM based SAFB method is applicable to ground wave propagation problem and has been validated against SSPE which is a very-well known and reliable algorithm for such problems. SAFBM is also convenient to take the affects of irregular terrain together with impedance boundary condition.

As an additional last word, it can be noted that widespread usage of numerical methods in simulating complex EM problems necessities us to be very cautious since the user must [23]

- Keep in mind that there is no generally applicable technique, so validity range and accuracy must be controlled.
- Well-understand the physics behind the mathematics and model of the simulator she uses
- Compare the simulation results with the reference preferable experimental data.

As a future work, atmosphere effects can be applied to SAFB method and in this way forward-backward method can model propagation better since atmospheric attenuation effects will be involved.

REFERENCES

[1] Meeks M.L., 1981. Radar Propagation At Low Altitudes, Artech House, Inc.

[2] Levy, M., 2000. Parabolic Equation Methods for Electromagnetic Propagation, IEE, Institution of Electrical Engineers, London.

[3] Tunç C.A., 2003. Application of spectral acceleration forward-backward method for propagation over terrain, The Institute of Engineering and Sciences of Bilkent University, MSc. Thesis, Ankara.

[4] Pino M. R., Burkholder R. J., and Obelleiro F., June 2002. Spectral Acceleration of The Generalized Forward-Backward Method, IEEE Trans. Antennas And Propagat., Vol. 50, Pp. 785-797.

[5] Wait, J.R., 1998. The Ancient and Modern History of EM Ground-Wave Propagation, *IEEE Transactions on Antennas and Propagation Magazine*, **40**, 7-24.

[6] Hall M.P.M., Barclay L.W., and Hewitt M.T., 1996. Propagation of Radiowaves, The Instituiton of Electrical Engineers, London.

[7] Rappaport, T.S., 1996. Wireless Communications, Prentice Hall, New Jersey.

[8] Akleman Funda, 2002. Time and Frequency Domain Numerical Modeling For Ground-Wave Propagation, *PhD Thesis,* Istanbul Technical University Institute Of Science And Technology, Istanbul.

[9] Sadiku, Matthew N.O, 1993. Numerical techniques in electromagnetics, CRC Press, Boca Raton

[10] R.F. Harrington, 1968. Field Computation by Moment Methods. Malabar, FL: Krieger.

[11] B.J. Strait, 1980. Applications of the Method of Moments to Electromagnetics

St. Cloud, FL: SCEEE Press.

[12] R.F. Harrington, 1992. "Origin and development of the method moments for field computation," in E.K. Miller et al., *Computational Electromagnetics.* New York: IEEE Press, pp. 43–47.

[13] R.F. Harrington, 1967 "Matrix methods for field problems," *Proc. IEEE,* vol. 55,no. 2, , pp. 136–149.

[14] M.M. Ney, 1985. "Method of moments as applied to electromagnetics problems," IEEE Trans. Micro. Theo. Tech., vol. MTT-33, no. 10, pp.972–980.

[15] A.T. Adams, 1974. "An introduction to the method of moments," Syracuse Univ., *Report RADC* TR-73-217, vol. 1, Aug.

[16] Chou H. T. and Johnson J. T., 1998. A novel acceleration for the computation of scattering from rough surfaces with the forward-backward method, Radio Sci., vol. 33, pp. 1277–1287,.

[17] Kouyoumjian R.G., and Pathak P.H., 1974. A uniform geometrical theory of diffraction for an edge in a perfectly conducting surface, Proc. IEEE, 62(11), pp. 1481-1461.

[18] Burkholder, R.J., and D.-H. Kwon, 1996. High-frequency asymptotic acceleration of the fast multiple method Radio Sci., 51(5), pp.1199-1026.

[19] Pino M. R., Landesa L., Rodriguez J. L., and Obelleiro F., 1999. The generalized forward-backward method for analyzing the scattering from targets on ocean-like rough surfaces", IEEE Trans. Antennas and Propagat., vol. 47, pp. 961-969.

[20] Chou H.-T. and Johnson J. T., 2000. Formulation of Forward-Backward Method Using Novel Spectral Acceleration for The Modeling Of Scattering From Impedance Rough Surfacessurface", IEEE Trans. Geosci. Remote Sensing, vol. 38, pp. 605-607.

[21] Barrios, A.E., 1994. A terrain parabolic equation model for propagation in the troposphere, *IEEE Transactions on Antennas and Propagation,* vol.42, 90-98.

[22] Sevgi, Levent, 1999. Elektromanyetik Problemler ve Sayısal Yöntemler, Birsen Yayıncılık, Istanbul.

[23] Sevgi, Levent, 2003. Complex Electromagnetic Problems & Numerical Simulation Approaches, IEEE Press - John Wiley and Sons Co., New Jersey.

0[24] Chou H.-T., 2000. Applications of forward-backward method in the fast analysis of large array problems", IEEE Antennas and Propagation Society International Symposium, vol. 4, pp. 2336-2339.

[25] M. Born and E. Wolf. ,1999. Principles of Optics. 7th edition, Pergamon Press.

BIOGRAPHY

A.Burçin NAİBOĞLU was born in Istanbul, Turkey in 1981. She finished Acıbadem Primary School in 1992 and Özel Doğuş High School in 1996. Later, she graduated from Özel Doğuş Science School in 1999. She received her BS degree in Telecommunication Engineering from Electrics and Communication Engineering Department of Yıldız Technical University in 2003. She is still working in NORTEL NETAŞ A.Ş. as a product support engineer.